https://doi.org/10.5194/acp-2019-881
Preprint. Discussion started: 18 November 2019

Atmospheric Chemistry and Physics Discussions

Detection and Attribution of Wildfire Pollution in the Arctic and Northern Mid-latitudes using a Network of FTIR Spectrometers and GEOS-Chem

Erik Lutsch[1], Kimberly Strong[1], Dylan B.A. Jones[1], Thomas Blumenstock[2], Stephanie Conway[1], Jenny A. Fisher[3], James W. Hannigan[4], Frank Hase[2], Yasuko Kasai[5], Emmanuel Mahieu[6], Maria Makarova[7], Isamu Morino[8], Tomoo Nagahama[9], Justus Notholt[10], Ivan Ortega[4], Mathias Palm[10], Anatoly V. Poberovskii[7], Ralf Sussmann[11], and Thorsten Warneke[10]

[1]Department of Physics, University of Toronto, Toronto, ON, Canada
[2]Karlsruhe Institute of Technology, IMK-ASF, Karlsruhe, Germany
[3]Centre for Atmospheric Chemistry, University of Wollongong, Wollongong, NSW, Australia
[4]National Center for Atmospheric Research, Boulder, CO, USA
[5]National Institute for Information and Communications Technology (NICT), Tokyo, Japan
[6]Institute of Astrophysics and Geophysics, University of Liège, Liège, Belgium
[7]St. Petersburg State University, St. Petersburg , Russia
[8]National Institute for Environmental Studies (NIES), Tsukuba, Japan
[9]Institute for Space-Earth Environmental Research (ISEE), Nagoya University, Nagoya, Japan
[10]Institute of Environmental Physics, University of Bremen, Bremen, Germany
[11]Karlsruhe Institute of Technology, IMK-IFU, Garmisch-Partenkirchen, Germany

Correspondence: elutsch@physics.utoronto.ca

Abstract. We present a multi-year time series of column abundances of carbon monoxide (CO), hydrogen cyanide (HCN), and ethane (C_2H_6) measured using Fourier transform infrared (FTIR) spectrometers at ten sites affiliated with the Network for Detection of Atmospheric Composition Change (NDACC). Six are high-latitude sites: Eureka, Ny-Ålesund, Thule, Kiruna, Poker Flat, and St. Petersburg , and four are mid-latitude sites: Zugspitze, Jungfraujoch, Toronto, and Rikubetsu. For each site, the inter-annual trends and seasonal variabilities of the CO time series are accounted for, allowing ambient concentrations to be determined. Enhancements above ambient levels were used to identify possible wildfire pollution events. Since the abundance of each trace gas emitted in a wildfire event is specific to the type of vegetation burned and the burning phase, correlations of CO to the long-lived wildfire tracers HCN and C_2H_6 allow for further confirmation of the detection of wildfire pollution, while complementary measurements of aerosol optical depth from nearby AERONET sites confirm the presence of wildfire smoke. A GEOS-Chem tagged CO simulation with Global Fire Assimilation System (GFAS) biomass burning emissions was used to determine the source attribution of CO concentrations at each site from 2003-2018. The influence of the various wildfire sources is found to differ between sites while North American and Asian boreal wildfires fires were found to be the greatest contributors to episodic CO enhancements in the summertime at all sites.

https://doi.org/10.5194/acp-2019-881
Preprint. Discussion started: 18 November 2019

Atmospheric Chemistry and Physics Discussions

1 Introduction

The Arctic is a major receptor for pollution from mid-latitude regions (Stohl et al., 2006; Law and Stohl, 2007; Shindell et al., 2008). Boreal wildfires are well known to have considerable impacts on the Arctic atmosphere and climate (Amiro et al., 2009; Warneke et al., 2009). Black carbon, also known as soot, is a strong contributor to global warming (Bond and Sun, 2005 and references therein). Black carbon in the Arctic has been studied extensively and it has been found that a substantial fraction of Arctic black carbon is transported from boreal wildfires (Stohl et al., 2006; Sharma et al., 2004, 2006; Wang et al., 2011; Sharma et al., 2013; Evangeliou et al., 2016; Winiger et al., 2019). Black carbon is well known to contribute to episodes of poor air quality and warm the atmosphere by absorbing radiation and covering snow- and ice-covered surfaces, indirectly exerting snow-albedo effects (McConnell et al., 2007; Ramanathan and Carmichael, 2008; Flanner, 2013). Boreal wildfires may also influence the carbon cycle (Conard and Ivanova, 1997; Schimel and Baker, 2002; Mack et al., 2011; Santín et al., 2015). In boreal wildfire events, considerable quantities of carbon monoxide (CO), carbon dioxide (CO_2) and methane (CH_4) are emitted (van der Werf et al., 2017). Boreal wildfire emissions of CO, CO_2 and CH_4 are dependent on burning phase, with greater emissions of CO_2 and CH_4 from flaming combustion, with CO emissions dominated by smoldering and residual phase combustion (Andreae and Merlet, 2001 and the references therein). Emissions of CO, CH_4, nitrogen oxides (NO_X) and volatile organic compounds (VOCs) from wildfires may then be oxidized to form CO_2 and ozone (O_3) (Levine, 2003).

Wildfires also contribute to the emission of a large number of reactive trace gas species, including VOCs, which promote the production of tropospheric O_3 and the formation of aerosols (Jaffe et al., 1999, 2004; Parrington et al., 2013; Wentworth et al., 2018) and therefore negatively impact air quality. Emissions of these species remain highly uncertain as a result of the dependence of emissions on fuel types (Andreae and Merlet, 2001; Akagi et al., 2011; Andreae, 2019); emissions from a particular event are strongly influenced by local meteorology, which has a direct influence on the burning phase and the emission of each species (Yokelson et al., 1996, 1999, 2003; Goode et al., 1999, 2000). Additionally, these reactive species are short-lived and are not easily measured downwind of the fire source. Wildfire plumes may be subject to long-range transport, and therefore it is necessary to measure the concentrations of these reactive trace gas species downwind in order to predict their influence on a global scale.

In the Northern hemisphere, boreal wildfires are a dominant source of biomass burning, brought on by persistent warm and dry conditions resulting in increased fire risk and ignition from lightning. Both periods of greater fire risk and lighting activity are expected to occur with increasing frequency at Northern high-latitudes as a result of anthropogenic-induced climate change (Krause et al., 2014; Veraverbeke et al., 2017). The magnitude and intensity of boreal wildfire activity are also projected to increase with future climate change (Amiro et al., 2009; Westerling et al., 2006; Flannigan et al., 2009; Wotton et al., 2010; Boulanger et al., 2014).

Quantifying the influence of biomass burning on the Arctic atmosphere requires long-term, dedicated measurements of the transported emissions in the Arctic. The Arctic is a difficult region to study as a result of the lack of dedicated measurement stations. Ground-based solar-absorption Fourier-transform infrared (FTIR) spectrometers have proven to be a useful tool for quantifying trace species abundances. The Network for the Detection of Atmospheric Composition Change (NDACC; www.

https://doi.org/10.5194/acp-2019-881
Preprint. Discussion started: 18 November 2019

Atmospheric Chemistry and Physics Discussions

ndacc.org; De Mazière et al., 2018) provides a global network of FTIR instruments that routinely measure the biomass burning tracers CO, hydrogen cyanide (HCN) and ethane (C_2H_6), in addition to a multitude of other trace gas species. The FTIR instruments of NDACC have previously been utilized to study biomass burning emissions. Zhao et al. (1997, 2000, 2002) identified Asian and Siberian biomass burning sources as major contribution to the measured concentrations of CO, HCN and C_2H_6 from ground-based FTIR measurements in Rikubetsu, Japan. Paton-Walsh et al. (2004, 2005, 2010) used solar-absorption FTIR measurements in Australia (Darwin (34°S, 150°E) and Wollongong (34°S, 150°E)) to quantify emissions of various trace gas species from Australian wildfires. Vigouroux et al. (2012) examined the influence of biomass burning in Southern Africa and Madagascar on FTIR measurements of HCN, C_2H_6, acetylene (C_2H_2), methanol (CH_3OH) and formic acid (HCOOH) at Reunion Island (21°S, 55°E) located in the Indian Ocean.

More recently, FTIR measurements in the Arctic have proven to be particularly useful, providing observational coverage of trace gas species where measurements from other platforms are scarce or non-existent. Viatte et al. (2013) identified enhancements of CO, HCN and C_2H_6 in FTIR measurements at Eureka (80°N, 86°W), Canada that were attributed to the 2010 Russian wildfires. A subsequent study by Viatte et al. (2014) demonstrated the utility of FTIR in measuring the biomass burning species C_2H_2, CH_3OH, HCOOH and formaldehyde (H_2CO) at Eureka. Analogous retrievals of these species were also performed for measurements from a second high-Arctic site at Thule (77°N, 69°W), Greenland and emission ratios and emissions factors were derived for these species from FTIR measurements at both Thule and Eureka by Viatte et al. (2015). Measurements of ammonia (NH_3) by solar-absorption FTIR spectroscopy was first demonstrated by Paton-Walsh et al. (2004) and later by Dammers et al. (2015). Lutsch et al. (2016) provided the first measurements of NH_3 in the high-Arctic and determined emission ratios and emissions for the 2014 Northwest Territories wildfires of Canada. The contribution of 2017 Canadian wildfires to NH_3 in the Arctic was examined using FTIR measurements at Eureka and Thule by Lutsch et al. (2019). The results of these studies highlight the ability of FTIR spectroscopy to measure a number of trace gas species, many of which are difficult to assess using satellite-based or other platforms.

However, each of these studies have only considered individual events or events that occurred in a short time series. Measurements using FTIR have been routinely made since the mid-1980s (Zander et al., 2008) and the number of measurement sites have increased since the inception of the Network for Detection of Stratospheric Change (NDSC; Kurylo, 1991) in 1991, which has been formally known as NDACC since 2005 (De Mazière et al., 2018). Several global FTIR sites have been measuring the biomass burning tracers CO, HCN and C_2H_6 over the last two decades. Yurganov (2004) identified enhanced CO columns in 1998 detected using FTIR measurements at several Northern mid- to high-latitude NDACC FTIR sites from 1996-2002. The 1998 CO anomaly was attributed to Siberian wildfires. A similar study by Yurganov et al. (2005) examined the 2002 and 2003 CO anomalies from Siberian wildfires using satellite-based, in situ and FTIR measurements in the Northern hemisphere. Currently, no study has explicitly examined the long-term and inter-annual variability of biomass burning species using FTIR measurements. A recent study by Petetin et al. (2018) investigated the impact of biomass burning on CO concentrations measured by the In-service Aircraft for a Global Observing System (IAGOS), which focused on airport clusters in Europe, North America, Asia, India and Southern Africa over the period 2002-2017. To our knowledge, no study of this kind has been performed for the Arctic and high-latitude regions.

https://doi.org/10.5194/acp-2019-881
Preprint. Discussion started: 18 November 2019

Atmospheric Chemistry and Physics Discussions

In this paper, the influence of wildfires on atmospheric composition from 2003-2018 is examined using FTIR measurements from three high-Arctic NDACC sites: Eureka, Canada; Ny-Ålesund, Norway and Thule, Greenland. Three Arctic sites are also included: Kiruna, Sweden; Poker Flat, Alaska and St. Petersburg , Russia. Additional measurements are obtained at four mid-latitude sites: Zugspitze, Germany; Jungfraujoch, Switzerland; Toronto, Canada and Rikubetsu, Japan. Potential wildfire pollution events are first identified in the CO time series at each site through the detection of anomalous enhancements of CO. For the CO enhancements detected at each site, enhancement ratios of HCN and C_2H_6 with respect to CO are calculated. Since CO, HCN and C_2H_6 are co-emitted from biomass burning sources, a strong linear correlation for the enhancement ratios of HCN and C_2H_6 indicate wildfire pollution events. The detection of wildfire pollution at each site was further confirmed using total aerosol optical depth (AOD) measurements from adjacent AERONET (Aerosol Robotic Network) sites. A GEOS-Chem tagged CO simulation from 2003-2018 was performed to identify the source attribution for the detected events at each FTIR site in addition to quantifying the contribution to CO from various biomass burning source regions.

The structure of this paper is summarized as follows. Section 2 provides an overview of each site and presents the retrieved products for CO, HCN and C_2H_6. Descriptions of the AERONET data and GEOS-Chem tagged CO simulation used in this study are also discussed in this section. The retrieved FTIR products for CO, HCN and C_2H_6 are presented and discussed in Section 3.1. The method for the detection of biomass burning pollution events is described in Section 3.2 and source attribution using the GEOS-Chem tagged CO simulation is shown in Section 3.3. The contribution of the GEOS-Chem CO tracers to FTIR measurements are presented and discussed in Section 3.4 and a comparison of the GEOS-Chem CO time series to FTIR measurements at all sites is shown in Section 3.5. The conclusions and summary of this study are highlighted in Section 4.

2 Methods

2.1 FTIR Sites and Retrievals

The NDACC FTIR sites included in this study were selected to provide coverage of high- and mid-latitude regions and are listed in Table 1. Due to the broad spectral range measured at high resolution, typically from 700-4400 cm^{-1} at 0.0035 cm^{-1} resolution, a multitude of trace gas species may be retrieved from solar-absorption FTIR measurements. Measurements of CO, HCN, and C_2H_6, all of which are standard products of the NDACC IRWG are the focus of this study. Retrievals of each species were performed by processing of solar-absorption spectra using the SFIT4 (https://wiki.ucar.edu/display/sfit4/) or PROFITT9 (Hase et al., 2004, for Kiruna and Zugspitze) retrieval algorithm which use the optimal estimation method (Rodgers, 2000) to obtain volume mixing ratio (VMR) profiles and integrated column abundances by iteratively adjusting VMR profiles to minimize the difference between the measured and calculated spectra (Pougatchev et al., 1995; Rinsland et al., 1998). Further details of the retrievals for each FTIR site are given in the references listed in Table 1.

https://doi.org/10.5194/acp-2019-881
Preprint. Discussion started: 18 November 2019

Atmospheric Chemistry and Physics Discussions

2.1.1 High-Arctic Sites

The highest-latitude FTIR site of NDACC is Eureka, located on Ellesmere Island in the Canadian Archipelago. It has been shown in previous studies that Eureka is regularly influenced by the transport of boreal wildfire emissions from North America and Asia (Viatte et al., 2013, 2014, 2015; Lutsch et al., 2016, 2019). Located approximately 500 km from Eureka is the site Thule on the Northwest coast of Greenland, which provides complementary measurements to Eureka as wildfire pollution events detected at Eureka are generally also observed in measurements at Thule (Viatte et al., 2015; Lutsch et al., 2019). Ny-Ålesund in Spitsbergen, Norway is the second highest-latitude FTIR site of NDACC. Ny-Ålesund is isolated from the direct influence of anthropogenic and wildfire emissions, but is affected by the long-range transport of pollution originating from Northern hemisphere mid-latitudes. For the purposes of this study, Eureka, Ny-Ålesund and Thule will be referred to as the "clean" high-Arctic (>75°N) sites because they are free of local pollution sources.

2.1.2 Arctic Sites

The Arctic sites are defined as those located between 60°N and 75°N, and include Poker Flat, Alaska; Kiruna, Sweden; and St. Petersburg, Russia. Poker Flat is strongly influenced by the transport of anthropogenic pollution from Siberia and Asia (Kasai et al., 2005b). Asian anthropogenic emissions have been found to be a predominant source of pollution in Alaska, with a greater influence in years with strong El Niño conditions (Fisher et al., 2010). Siberian wildfires are a substantial source of summertime pollution in Alaska (Jaffe et al., 2004; Warneke et al., 2009) in addition to local wildfires within the boreal forests of Alaska. It should be noted that for this reason, and the dependence of FTIR measurements on clear-sky conditions, smoke plumes within Alaska may prevent measurements by FTIR. As a result, summertime measurements at Poker Flat can be sparse.

Kiruna is mainly influenced by anthropogenic emissions from mid-latitude Europe; however, aerosol smoke layers from injection of Canadian wildfire emissions into the lower stratosphere have been identified in the past at Kiruna (Fromm et al., 2000). Similarly, the urban site of St. Petersburg would be most sensitive to local sources within Europe. Both Kiruna and St. Petersburg may sample the long-range transport of boreal Asian plumes that could circle the Northern Hemisphere (Damoah et al., 2004), although such plumes would be well aged and diluted. Through injection of wildfire emissions into the upper troposphere and lower stratosphere, North American boreal wildfire plumes may be efficiently transported to Europe (Khaykin et al., 2018; Hu et al., 2019). Although the effects of the long-range transport of wildfire emissions on air quality are likely to be minimal, they can have an influence on tropospheric composition of long-lived species.

2.1.3 Alpine Sites

Both Zugspitze and Jungfraujoch are considered clean Alpine sites, isolated from local pollution sources and therefore provide measurements that are representative of background concentrations of central Europe (Franco et al., 2015). For the purpose of this study, as the result of the close proximity between the two sites (∼200 km), Zugspitze and Jungfraujoch are considered to be complementary to one another. Differences in measured column amounts between the two sites as a result of long-range transport are likely due to their altitude differences, 2964 m a.s.l. and 3580 m a.s.l. for Zugspitze and Jungfraujoch, respectively.

https://doi.org/10.5194/acp-2019-881
Preprint. Discussion started: 18 November 2019

Atmospheric Chemistry and Physics Discussions

It has been previously shown that Zugspitze is weakly influenced by nearby pollution sources, while Jungfraujoch is considered a remote site, mainly influenced by long-range transport (Henne et al., 2010). However, as a result of the high altitudes of these sites, the measured composition is largely driven by long-range transport in the mid to upper troposphere.

2.1.4 Mid-latitude Sites

Toronto, an urban site, is most sensitive to local pollution sources in southeast Canada and the United States (Whaley et al., 2015) and periodically subject to wildfire pollution episodes as demonstrated by Griffin et al. (2013); Whaley et al. (2015). Rikubetsu, located in Hokkaido, Japan, is free of considerable local anthropogenic pollution sources, with contributions of CO mainly due to transported Asian anthropogenic emissions (Zhao et al., 2000). In the summertime, Rikubetsu is influenced by the transport of biomass burning pollution from within Asia (Li et al., 2000), while the region of Hokkaido is often affected by pollution episodes from Siberian wildfires of boreal Asia (Jeong et al., 2008; Tanimoto et al., 2000; Yasunari et al., 2018).

2.2 GEOS-Chem

To interpret the influence of anthropogenic, chemical, and biomass burning sources on CO columns at each FTIR site, the GEOS-Chem chemical transport model is used (http://geos-chem.org/;Bey et al., 2001b) in a tagged simulation of CO at a horizontal resolution of $2^\circ \times 2.5^\circ$ with 47 vertical hybrid levels. GEOS-Chem version 12.1.1 (The International GEOS-Chem User Community, 2018) was used and driven by global meteorological inputs from the MERRA-2 (Modern-Era Retrospective Analysis for Research and Applications, Version 2; Gelaro et al., 2017) from the NASA Global Modeling and Assimilation Office (GMAO). MERRA-2 is produced with the GMAO/GEOS-5 (Goddard Earth Observing System) Data Assimilation System Version 5.12.4. The GEOS-Chem simulation was initialized with a 1-year spin-up from 1 January 2002 to 1 January 2003. Chemical and transport operator time-steps of 1 hr and 10 min, respectively, were used.

Biomass burning emissions are from GFASv1.2 (Global Fire Assimilation System, Kaiser et al., 2012; Giuseppe et al., 2018) which assimilates Moderate Resolution Imaging Spectroradiomter (MODIS) burned area and fire radiative power (FRP) products to estimate emissions for open fires. GFASv1.2 emissions have a $0.1^\circ \times 0.1^\circ$ horizontal resolution with 3-hourly temporal resolution. GFAS was chosen for the availability of emissions over the analysis period from 2003-2018. Global anthropogenic emissions are provided from the EDGARv4.3.1 (Emission Database for Global Atmospheric Research, Crippa et al., 2016) emissions inventory, overwritten by regional emission inventories in the Northern hemisphere as described in Fisher et al. (2010). Biogenic emissions of precursor VOCs are from the Model of Emissions of Gases and Aerosols from Nature (MEGANv2.1; Guenther et al., 2012) and biofuel emissions are taken from Yevich and Logan (2003).

The main loss mechanism for CO is from photochemical oxidation by the hydroxyl radical (OH). The OH fields are prescribed in the tagged CO simulation and were obtained from the TransCom experiment (Patra et al., 2011) which implements semi-empirically calculated tropospheric OH concentrations from Spivakovsky et al. (2000) to reduce the high bias of OH from the GEOS-Chem full-chemistry simulation (Shindell et al., 2006). Surface emissions in GEOS-Chem are released within the boundary layer, and boundary layer mixing is implemented using the non-local mixing scheme of Holtslag and Boville (1993). Biomass emissions are released by uniformly distributing emissions from the surface to the mean altitude of maxi-

https://doi.org/10.5194/acp-2019-881
Preprint. Discussion started: 18 November 2019

Atmospheric Chemistry and Physics Discussions

mum injection based on the injection height information as described in Rémy et al. (2017) which includes an injection height parameterization by Sofiev et al. (2012) and a plume rise model by Freitas et al. (2007).

GEOS-Chem version 12.1.1 tagged CO simulation includes the improved secondary CO production scheme of Fisher et al. (2017), which assumes production rates of CO from CH_4 and NMVOC oxidation from a GEOS-Chem full-chemistry simulation therefore reducing the mismatch between the CO-only simulation and the full-chemistry simulation. The anthropogenic source regions are shown in Figure 1, while biomass burning source regions are implemented following the standard GFED (Giglio et al., 2013) regions and are also shown in Figure 1.

2.3 AERONET

The Aerosol Robotic Network (AERONET; https://aeronet.gsfc.nasa.gov; Holben et al., 1998) is a federation of ground-based remote sensing aerosol networks established by NASA and PHOTONS (PHOtométrie pour le Traitement Opérationnel de Normalisation Satellitaire; Univ. of Lille 1, CNES, and CNRS-INSU). AERONET consists of a network of CIMEL sun photometers which provides globally distributed observations of spectral aerosol optical depth (AOD). At each AERONET site, observations are recorded every 15 minutes and are cloud screened. Inversion of aerosols products and cloud screening for the AERONET Version 3 database are described in (Giles et al., 2019). AERONET sites selected for this study were based on the availability of data during the operational period of the FTIR instruments and proximity to the FTIR site. The selected AERONET sites nearest to the NDACC FTIR sites are listed in Table 1.

3 Results & Discussion

3.1 Retrieved FTIR Products

3.1.1 Time Series

The weekly-mean time series of CO, HCN and C_2H_6 tropospheric partial columns for each site are shown in Figures 2, 3 and 4 respectively. The tropospheric partial columns are the integrated column amounts from the surface to an altitude of 12.71 km at each site. In this study, all presented column amounts correspond to this partial column for CO, HCN and C_2H_6. The weekly mean is taken over all years of measurements for the respective species at each site, while the shaded region indicates a 1σ deviation from the mean. For all sites, the seasonal cycle of CO shows a maximum in winter and early spring (February-March), with decreasing total columns through the spring. The main sources of CO are the combustion of fossil fuels and biomass burning, while oxidation of VOCs and CH_4 are also a considerable source (Holloway et al., 2000). The main sink of CO is due to reaction with OH, leading to a lifetime of approximately 1-2 months (Bey et al., 2001a). In winter and spring months, decreased sunlit hours limits OH production by photolysis of ozone, therefore minimizing the loss of CO. The seasonal cycle of OH largely drives the seasonal variations of CO. Transport of CO from mid-latitude to high-latitude regions also contributes to the seasonal cycle as the isentropic transport is greater in the winter and spring months (Klonecki,

https://doi.org/10.5194/acp-2019-881
Preprint. Discussion started: 18 November 2019

Atmospheric Chemistry and Physics Discussions

2003; Stohl et al., 2006). Furthermore, the stronger seasonal cycle of OH production also contributes to the greater seasonal amplitudes at high latitudes as observed in Figure 2.

Enhanced tropospheric columns of CO are observed in the summertime, mainly in July-September at all sites as illustrated in Figure 2 as a result of the hemispheric influence of boreal wildfires (Honrath, 2004). These enhancements are most pronounced at the clean high-Arctic sites of Eureka and Thule, which are strongly influenced by boreal fires in North America and Asia. Similar enhancements are also observed at the other Arctic sites of Ny-Ålesund and Kiruna, but are not as pronounced, which is partly due to the longer transport times to these sites. Ny-Ålesund also exhibits an increase in CO beginning in August as a result of the accumulation of CO from Northern Hemisphere biomass burning sources. Poker Flat, located in the boreal forests of Alaska is greatly influenced by boreal wildfire emissions in these regions; however, in many instances these events result in smokey conditions that prevent FTIR measurements. As a result detection of enhancements at Poker Flat are likely to be underestimated due to the strong influence of wildfire smoke.

A slight increase in CO concentrations is observed at Zugspitze and Jungfraujoch as a result of the long-range transport of boreal wildfire emissions. Emissions from these events are often lofted into the free troposphere where long-range transport is favoured (Jaffe et al., 2004; Val Martin et al., 2006). However, the transport of emissions over continental scales results in the dilution of the smoke plume and therefore, the enhancements observed at Zugspitze and Jungfraujoch are not as pronounced as for the other sites.

St. Petersburg and Toronto are urban sites that are strongly influenced by local anthropogenic sources, but enhanced columns of CO are observed in July and August as a result of the boreal wildfire influence. Rikubetsu is strongly affected by anthropogenic CO sources from Asia, resulting in the large variability of CO (Zhao et al., 1997, 2002). The greatest enhancements at Rikubetsu are observed in July and August, due to boreal Asian wildfires in Siberia.

HCN has a long atmospheric lifetime ranging from days to months, while its dominant source is due to biomass burning emissions (Li et al., 2000, 2003, 2009). Plant and fungal emissions represent a minor source of HCN, while dry deposition to the ocean and oxidation by OH are the main sinks (Cicerone and Zellner, 1983). As a result, HCN will accumulate in the Northern hemisphere in the summer months due to the influence of wildfire and biogenic emissions. The seasonal cycle of HCN peaks in the summer months with low total columns in the winter and fall as illustrated in Figure 3. A sharp maximum is observed in August at the high-Arctic sites (Eureka, Thule and Ny-Ålesund) due to activation of its biogenic sources and the onset of wildfire emissions. A similar increase in the HCN total columns is observed at the high-latitude sites (Kiruna, Poker Flat and St. Petersburg), although not as pronounced. For Toronto, enhanced total columns are also observed in August due to wildfires, consistent with the CO time series. Rikubetsu shows the greatest concentrations of HCN in the spring in May, with a secondary peak in August. The springtime enhancements of HCN are due to the earlier onset of East and Southeast Asian biomass burning, which occurs annually from March to May (Streets et al., 2003).

The seasonal cycle of C_2H_6 is similar to that of CO, as shown in Figure 4. The primary sources of C_2H_6 include natural gas production, biofuel use and biomass burning (Rudolph, 1995; Logan et al., 1981; Xiao et al., 2008). The main loss of C_2H_6 is due to reaction with OH, resulting in an average lifetime of approximately three months (Xiao et al., 2008). The summertime wildfire influence of C_2H_6 is less pronounced than for CO and HCN. Enhancements of C_2H_6 are particularly evident at Eureka

https://doi.org/10.5194/acp-2019-881
Preprint. Discussion started: 18 November 2019

Atmospheric Chemistry and Physics Discussions

and Thule, due to the generally clean background of these sites, while wildfire enhancements of C_2H_6 are not evident at the other sites due to the influence of local sources in addition to dilution of the plume during long-range transport. Therefore, C_2H_6 enhancements due to wildfire pollution are not generally apparent over background concentrations. Additionally, the emissions of C_2H_6 are an order of magnitude lower than those of HCN for boreal forest, temperate forests and peatland burning sources (Andreae and Merlet, 2001; Akagi et al., 2011; Andreae, 2019).

3.1.2 Volume Mixing Ratio Profiles

The VMR profiles of CO, HCN and C_2H_6 for all sites are shown in Figures 5, 6 and 7. In all cases, the profiles of each species are similar between sites and tend not to show drastic differences. It should be noted, that these profiles do not represent the true atmospheric profile of the species due to limited vertical resolution of the measurement, which is inherent in remote sensing measurements of this kind. The retrieved profiles generally follow a similar shape to the a priori profile, where deviations from the a priori are a result of the measurement. The information content of the retrieval will be discussed in the following section. In general, the profiles of all species exhibit greatest variability in the troposphere due to the abundance of these species in this region as these species are considered to be primarily tropospheric. The the tropospheric column of CO, HCN and C_2H_6 comprise, on average, greater than approximately 90% of the total column for CO, 95% for HCN, and 98% for C_2H_6.

The VMR profiles of CO (Figure 5) exhibit the greatest values in the lower free troposphere (surface-6 km) at all sites, with values ranging from approximately 120-170 ppbv, with greater concentrations at the polluted sites of Toronto, St. Petersburg and Rikubestu. These sites also illustrate a peak CO concentration at the surface layer due to the influence of local or nearby emissions. For Rikubetsu, a slight increase in concentration from the surface ($\sim$170 ppbv) to 1 km ($\sim$175 ppbv) with concentrations decreasing with altitude as a result of the transport of CO in the free troposphere from nearby Asian sources is observed. Decreasing concentrations and reduced variability of the retrieved profiles with altitude is observed at all sites as transported CO is generally well mixed. Poker Flat shows greatest variability of the CO profiles due to the transport of Asian pollution in the spring and wildfires in Eurasia and Alaska in the summer (Kasai et al., 2005b).

The VMR profiles of HCN (Figure 6) are variable amongst sites, with surface-layer concentrations ranging from $\sim$190-310 pptv. For most sites, a peak in the concentration is observed between 6-10 km, with decreasing concentrations above. The HCN vertical profiles generally show increasing concentrations from the surface to the mid-troposphere and decreasing concentrations above. The urban sites, St. Petersburg and Toronto show decreasing concentrations from the surface due to the influence of local anthropogenic sources, mainly automobile use (Baum et al., 2007; Moussa et al., 2016). Accumulation of HCN in the upper troposphere is the result of its long lifetime and limited dry deposition to the ocean (Singh, 2003). This is most evident at Ny-Ålesund, which is isolated from local sources and illustrates an upper-troposphere peak between 7-9 km, with a concentration of approximately 330 pptv.

The VMR profiles of C_2H_6 (Figure 7) follow a similar vertical structure to that of CO as a result of their common sources. For the urban sites, St. Petersburg and Toronto, the concentration is greatest at the surface layer, approximately 2 ppbv and 2.4 ppbv respectively, as a result of local sources. Rikubetsu shows a peak near 1.7 km of 1.6 ppbv, due to the transport of emissions in the free troposphere from nearby Asian sources. For Arctic sites, Eureka, Ny-Ålesund, Kiruna and Poker Flat,

https://doi.org/10.5194/acp-2019-881
Preprint. Discussion started: 18 November 2019

Atmospheric Chemistry and Physics Discussions

C_2H_6 profiles show a broad peak in the free troposphere, generally between 1-7 km, which is indicative of the long-range transport of pollution.

3.1.3 Averaging Kernels

The averaging kernel characterizes the vertical information content of the retrievals as described in Rodgers (2000). We consider the total column averaging kernel ($\mathbf{a}$), rather than the averaging kernel matrix ($\mathbf{A}$). We define the total column averaging kernel vector:

$$\mathbf{a} = \mathbf{C}^T\mathbf{A}, \tag{1}$$

where $\mathbf{C}$ is the total column operator in units of molecules cm^{-2} and T denotes the transpose. The VMR averaging kernel matrix $\mathbf{A}$ is in VMR/VMR units. The total column averaging kernel may be normalized:

$$\hat{a}_i = a_i/C_i, \tag{2}$$

where i is the index of the ith level of the FTIR vertical retrieval grid. The normalized total column averaging kernel ($\hat{\mathbf{a}}$) is unitless and represents the sensitivity to a change in partial column for the vertical level i. The normalized total column averaging kernel may then be applied to the partial column profile to obtain the smoothed column, as will be discussed further in Section 3.5. For this purpose, normalized total column averaging kernel values near unity throughout the troposphere are desired, which would minimize biases due to differences in the vertical sensitivities when computing the ratios of columns of different species, as will be done in the following section.

The mean normalized total column averaging kernels, referred to as simply the total column averaging kernel hereinafter, for CO, HCN and C_2H_6 are shown in Figure 8. For all sites, the total column averaging kernels of CO show a value near 1 throughout the troposphere, with a slight decrease to values below unity above 5 km. For HCN, the total column averaging kernels increase from the surface, with maximum values in the upper troposphere. The total column averaging kernels of C_2H_6 show similar structure to HCN, with maximum values in the mid to upper troposphere. For all sites, it can be concluded that CO retrievals exhibit minimal sensitivity bias in the troposphere. For HCN and C_2H_6, the total column averaging kernel is greatest in the upper troposphere.

For all species and sites, the total column averaging kernels are not highly variable in time. The variability of the total column averaging kernel is mainly due the changes in the vertical distribution of the species. In particular, total column averaging kernel values generally increase with greater concentration of the species. There is some dependence on the solar zenith angle (SZA) of the measurement which varies seasonally, as the SZA is related to the sampled slant path through the atmosphere. At high SZAs, the longer slant path results in greater degrees of freedom for signal (DOFS), and hence greater averaging kernel values. The a priori covariance matrix, which is site and species dependent, also influences the total column averaging kernel.

https://doi.org/10.5194/acp-2019-881
Preprint. Discussion started: 18 November 2019

Atmospheric Chemistry and Physics Discussions

3.2 Detection of Wildfire Pollution Events

As was illustrated in Section 3.1.1 and Figure 2, a seasonal cycle of CO is observed, with the amplitude varying by site location. Over a long time series, CO may be subject to inter-annual trends as a result of changing emissions of CO and its precursors. Additionally, non-clear sky conditions and instrument downtime result in periodic gaps in measurements and non-uniform time intervals between measurements. As a result of these factors it can be difficult to determine baseline or ambient concentrations of CO and therefore to detect enhancements of CO in the FTIR time series. To mitigate these influences, we account for the seasonal cycle and inter-annual variability of the CO time series measured at each FTIR site following Thoning et al. (1989):

$$C(t) = a_0 + a_1 t + a_2 t^2 + \sum_{n=1}^{4} b_n \cos(2\pi n t) + c_n \sin(2\pi n t), \tag{3}$$

where C is the column CO concentration as a function of time t. The coefficients a_n account for the inter-annual trends of CO, while the fourth-order Fourier series with coefficients b_n and c_n captures the seasonal cycle of CO. The choice of order for both the polynomial and Fourier components of the fits were limited to third and fourth order following past studies (Thoning et al., 1989; Zellweger et al., 2009).

Enhancements in CO are identified following Zellweger et al. (2009). First, the fitted function is subtracted from the data to yield the residual. Assuming a normal distribution of baseline values around the fitted function, the negative residual is mirrored into the positive direction. Enhanced CO measurements are defined as those greater than a specified threshold of the mirrored residual above the fitted function. The threshold is defined as a multiple of the standard deviation σ of the mirrored negative residual as listed in Table 3. The threshold is 1σ for all sites, with the exception of Rikubetsu where a 2σ standard deviation was used as a result of the greater variability CO due to nearby Asian sources. The selected values are listed in Table 3.

The detected CO enhancements at each site are then binned by date to define individual events. The time window selected for binning is listed in Table 3 for each site and based on the measurement density at the respective site. Enhanced CO measurements separated in time by this duration are binned as separate events, while consecutive measurements within this time window are defined as a single event. Binning events minimizes the influence of varying plume composition, and also separates CO enhancements that may not be of wildfire origin. This is particularly important for the calculation of the enhancement ratio which will be described below. Longer separation times are selected for sites that are likely to be continually influenced by wildfire emissions. These values are summarized in Table 3. At this stage, no attribution of the detected CO enhancements to any source has been performed and these enhanced periods simply indicate possible pollution events.

To isolate potential wildfire pollution events, we exploit the fact that trace gas emissions from wildfires are specific to burning phase and vegetation type (Ward and Hardy, 1991; Yokelson et al., 1999; Andreae and Merlet, 2001; Yokelson et al., 2009; Akagi et al., 2011; Urbanski, 2013, 2014) and therefore it would be expected that emissions of CO, HCN and C_2H_6 originating from a wildfire source would be correlated within a plume. Emissions at the fire source are characterized by the emission ratio (ER; Andreae and Merlet, 2001; Akagi et al., 2011) relative to CO, which quantifies the amount of a trace gas species emitted

https://doi.org/10.5194/acp-2019-881
Preprint. Discussion started: 18 November 2019

Atmospheric Chemistry and Physics Discussions

relative to the amount of CO emitted. Since FTIR observations of this kind are measuring the emissions downwind of the source, the enhancement ratio (EnhR; Lefer et al., 1994) is considered:

$$\mathrm{EnhR_X} = \mathrm{slope}\left(\frac{[\mathrm{X}]}{[\mathrm{CO}]}\right)_{\Delta t=1\mathrm{hr}} \tag{4}$$

where [X] is the column of the trace gas of interest, and [CO] is the column of CO. The enhancement ratio is related to the emission ratio with the influence of plume aging by chemical loss, deposition and dilution of the plume during transport. Lifetimes of CO, HCN and C_2H_6 are generally longer than plume transport times which range from several days to approximately two weeks (Damoah et al., 2004) and therefore these species do not undergo chemical considerable chemical loss. Furthermore, we do not take into account the background concentrations which can cause uncertainty in interpreting the enhancement ratio as the ambient conditions are likely to vary along the plume trajectory (Yokelson et al., 2013).

To calculate the enhancement ratios from the FTIR measurements, the detected CO enhancements for each event were paired with the nearest HCN and C_2H_6 measurement taken within 1 hr. A 1-hr time interval was chosen to maximize the number of pairs since CO, HCN and C_2H_6 are measured using different spectral filters and hence the measurements do not occur simultaneously. For events with paired measurements of HCN or C_2H_6 with CO that are fewer than 5, the event is omitted. Setting a minimum number of pairs mitigates the potential of false detections as a result of spurious measurements.

The unified least-squares fitting procedure of York et al. (2004) which accounts for errors in both the ordinal and abscissa coordinates was used to determine a linear regression for the paired fire-affected measurements. The slope of the linear regression is the enhancement ratio for the respective species defined in Equation 4. To identify enhancements due to wildfire pollution events, we require that the correlation coefficient (r) be greater than or equal to 0.5 for both the enhancement ratios HCN and C_2H_6, unless otherwise stated, as summarized in Table 3.

HCN is retrieved from NDACC Filter 2 measurements, which is generally covered at least once per measurement sequence of all filters. Similarly, C_2H_6 is retrieved through filter NDACC filter 3. All filters have a different response to the input solar beam intensity and therefore, the measurement noise may vary between subsequent measurements of different filters. For this reason, adequate signal may not be obtained through all filters in the case of partially cloudy or non-clear sky conditions. It was found that for all sites, with the exception of Jungfraujoch, there are a greater number of CO measurements than HCN or C_2H_6. Because of this non-uniform distribution of measurements, the number of detected wildfire events is limited by the number of paired measurements for HCN or C_2H_6 with CO. For this reason, for Ny-Ålesund, Poker Flat and Rikubetsu, the enhancement ratio correlation criteria (shown in Table 3) were omitted, resulting in a lower confidence for the detected wildfire pollution events. However, for detected events at these sites, the adjacent AERONET sites provide additional evidence for the detection of wildfire emissions if the measured AOD is simultaneously enhanced with CO as shown in Figure 9. Furthermore, the GEOS-Chem tagged CO simulation provides further confidence in the detected wildfire pollution events as discussed in the following section.

https://doi.org/10.5194/acp-2019-881
Preprint. Discussion started: 18 November 2019

Atmospheric Chemistry and Physics Discussions

3.3 Source Attribution

A GEOS-Chem tagged CO simulation was performed as described in Section 2.2 for the time period of 2003-2018, giving 6-hourly instantaneous VMR profiles of the tracers listed in Table 2. The GEOS-Chem simulation provides a means of evaluating the source attribution for the detected wildfire pollution events in the FTIR time series. Source attribution is performed as follows. First, the GEOS-Chem CO VMR profiles in the grid box containing the respective FTIR site were converted to partial column profiles and linearly interpolated and regridded onto the FTIR vertical retrieval grid. This was necessary in order to account for the differences in the surface levels of the model and the FTIR sites (Barret et al., 2003). For each of the detected events, the period of fire-affected measurements is considered. For this fire-affected window, we define the first-order rate of change of the CO partial column contribution for each of the GEOS-Chem tagged biomass burning CO tracers:

$$\frac{\mathrm{d}[\mathrm{CO}]_\mathrm{X}}{\mathrm{d}t} = \frac{[\mathrm{CO}]_\mathrm{X}(t_i) - [\mathrm{CO}]_\mathrm{X}(t_{i-1})}{t_i - t_{i-1}}, \tag{5}$$

where $[\mathrm{CO}]_\mathrm{X}$ is the column (in molec cm^{-2}) of the CO tracer X and t_i is the time of the GEOS-Chem timestep. Within a wildfire pollution event, it is expected that a rapid increase of the CO contribution would be observed, resulting in a positive value $d[\mathrm{CO}]_\mathrm{X}/dt$. Similarly, as the plume passes or dissipates, a negative value of $d[\mathrm{CO}]_\mathrm{X}/dt$ would be observed. Considering this, the so-called impulse is then defined:

$$I_\mathrm{X} = \int_{t_0}^{t_f} \left| \frac{\mathrm{d}[\mathrm{CO}]_\mathrm{X}}{\mathrm{d}t'} \right| \mathrm{d}t' \tag{6}$$

where t_0 and t_f correspond to the start time and end times of the detected event. The absolute value is used since we do not discriminate against positive of negative rates of change. Since the model output timesteps are discrete and constant, using the definition of Equation 5, Equation 6 may be approximated as:

$$I_\mathrm{X} = \sum_{i=1}^{N} |[\mathrm{CO}]_\mathrm{X}(t_i) - [\mathrm{CO}]_\mathrm{X}(t_{i-1})| \tag{7}$$

where N is the number of GEOS-Chem output timesteps for the detected FTIR event from t_0 and t_f. The result of Equation 7 can be easily interpreted. For a wildfire event, the concentration would rapidly increase as the plume approaches the FTIR site and rapidly decreasing CO concentrations as the plume passes. In contrast, anthropogenic, chemical or biogenic sources of CO are less likely to contribute to episodic enhancements, as these sources tend to vary on seasonal timescales and are more likely to contribute to background concentrations of CO rather than anomalous enhancements. However, the transport of anthropogenic emissions in the winter and spring may result in episodic pollution events. Detection of anthropogenic pollution events was mitigated by the use of the correlation criteria for the enhancement ratios of HCN and C_2H_6 as mentioned previously. For Ny-Ålesund, Poker Flat and Rikubetsu where no correlation criteria was used, winter and spring anthropogenic events were identified and removed based on a qualitative assessment of the GEOS-Chem and AERONET AOD time series.

https://doi.org/10.5194/acp-2019-881
Preprint. Discussion started: 18 November 2019

Atmospheric Chemistry and Physics Discussions

The value of I_X would be greatest for the GEOS-Chem tagged CO tracer contributing to the episodic enhancement detected by the FTIR instrument, and for the reasons stated above, is likely to be of wildfire origin. The source of the detected FTIR enhancement therefore corresponds to the GEOS-Chem tagged CO tracer for which I_X from Equation 7 is a maximum. The source attribution for the detected wildfire pollution events in the FTIR time series is illustrated in Figure 10.

The mean enhancement ratios of HCN and C_2H_6 are summarized in Table 5 for the detected wildfire pollution events from BONA and BOAS at all sites. Similar enhancement ratios of HCN and C_2H_6 are observed at Eureka and Thule for both BONA and BOAS. This similarity is expected due to the close proximity of these sites. For Kiruna, slightly lower mean enhancement ratios of HCN were observed of 0.005 for both BONA and BOAS. The enhancement ratio of C_2H_6 at Kiruna is greater than Eureka and Thule, which likely represents the longer travel times of the plume resulting in the dilution of the plume with the background, which can be interpreted as follows. Assuming lifetimes of CO, HCN and C_2H_6 of 30, 75 and 45 days following Viatte et al. (2013, 2015) and Lutsch et al. (2016), the enhancement ratio (EnhR) is given with respect to the emission ratio (ER):

$$\mathrm{EnhR}_X = \mathrm{ER}_X \cdot \frac{\exp\left(-\frac{t}{\tau_X}\right)}{\exp\left(-\frac{t}{\tau_{CO}}\right)}. \tag{8}$$

It is easily seen from Equation 8 that the enhancement ratios of HCN and C_2H_6 would increase with longer plume travel times t. For example, assuming a 7 day travel time, the enhancement ratios of HCN and C_2H_6 would be a factor of 1.15 and 1.08 greater than their respective emission ratio. For a 14 day travel time, the enhancement ratios of HCN and C_2H_6 would increase by a factor of 1.32 and 1.16, respectively, from their respective emission ratios. However, this is neglecting the influence of plume dilution. With longer travel times, the plume is likely to mix with the background resulting in the enhancement ratios tending to background values. Therefore, the enhancement ratio of C_2H_6 would likely be greater than the enhancement ratio of HCN as a result of the greater mean columns of C_2H_6 in comparison to HCN observed at all sites, as illustrated in Figures 3 and 4.

With the exception of Toronto, which is likely influenced by local HCN sources, the greatest HCN enhancement ratios are observed at Eureka and Thule, with greater values for the BOAS events, 0.008 and 0.009 for Eureka and Thule, respectively. It is possible that this could reflect the greater HCN emissions of BOAS due to the substantial fraction of peat burning from these events (Yurganov et al., 2011; R'Honi et al., 2013). Lower enhancement ratios of HCN are observed at all other sites (except Toronto) for both BONA and BOAS sources. The lower enhancement ratios of HCN likely reflect the longer travel times to these sites and the dilution of the plume as described above.

Episodic wildfire pollution events at all sites are attributed to either BONA or BOAS sources, with two detected events from SEAS at Jungfraujoch. Temporal correlation of events amongst all sites is observed, with events occurring near in time at different sites is attributed to the same source. Particularly evident are the 2012 Siberian wildfires (Kozlov et al., 2014; Teakles et al., 2017) observed at several sites and attributed to BOAS. Similarly, the 2017 Canadian wildfires (Khaykin et al., 2018; Peterson et al., 2018; Kirchmeier-Young et al., 2019; Lutsch et al., 2019) are also observed at a number of sites. Although,

https://doi.org/10.5194/acp-2019-881
Preprint. Discussion started: 18 November 2019

Atmospheric Chemistry and Physics Discussions

the majority of detected events from 2003-2018 are attributed to BOAS, from 2013-2018 there is an observed increase in the number of events attributed to BONA, with 24 BONA and 14 BOAS events detected during this period amongst all sites. Prior to 2013, 17 BONA and 37 BOAS events were detected. The recent increase in BONA events could be indicative of changes in large-scale climatic patterns (Macias Fauria and Johnson, 2008) resulting in an increase in lighting-induced wildfires (Macias Fauria and Johnson, 2006; Veraverbeke et al., 2017). However, this apparent increase in BONA events does not take into account the possibility of missed detections due to instrument downtime or cloudy sky conditions. Contributions of the biomass burning source regions to CO tropospheric columns at each site will be discussed in the following section.

3.4 Wildfire Contribution to CO

The GEOS-Chem tagged CO simulation provides a means of evaluating the contribution of CO from anthropogenic, chemical and biomass burning sources to the measured CO columns at each FTIR site. Figures 12 to 15 show the daily-averaged GEOS-Chem and FTIR CO tropospheric columns (surface-12.71 km) for the simulation period from 2003-2018. The relative contribution of biomass burning tracers are also shown. Biomass burning tracers with a mean contribution of less than 3% are not shown. For all GEOS-Chem tagged CO tracers, the partial column profile was linearly interpolated onto the FTIR retrieval grid to account for the differences in surface elevation of the model and FTIR sites.

For all sites, the oxidation of CH_4 is the greatest contribution to the tropospheric CO column as illustrated in Figure 11. The magnitude of this source is similar amongst all sites, with the exception of Zugspitze and Jungfraujoch due to their high altitude. Anthropogenic Asian CO sources exhibit the greatest seasonal amplitude at all sites, due to the magnitude of the emissions and the influence of seasonally variable transport (Klonecki, 2003; Stohl et al., 2006; Fisher et al., 2010). European and North American anthropogenic sources show a similar seasonal cycle but smaller in amplitude in comparison to the Asian source. Of note, at Zugspitze and Jungfraujoch, comparable contributions from anthropogenic sources in Asia, North America, Europe and the rest of the world are observed. The oxidation of NMVOCs is a considerable source at all sites, with little seasonal dependence. A slight increase in the NMVOC contribution is observed in the summertime, particularly in July and August, as a result of emissions of NMVOC from biogenic sources and wildfires (Guenther et al., 2000; Wentworth et al., 2018).

Biomass burning sources of CO exhibit the greatest differences amongst sites as seen in Figure 11. For most sites, the onset of the biomass burning contribution begins in May with a maximum in August. Similar to the anthropogenic influence, Zugspitze and Jungfraujoch are generally isolated from the direct influence of biomass burning emissions and only show a minor enhancement in the summer. For Rikubetsu, the onset of the biomass burning contributions is observed earlier than for the other sites beginning in March as a result of the influence of Asian biomass burning sources (CEAS, SEAS and EQAS), with slight influence in the summer for boreal emissions from BOAS. The contributions of the biomass burning sources to each site with respect to the results of Section 3.3 are discussed below.

https://doi.org/10.5194/acp-2019-881
Preprint. Discussion started: 18 November 2019


Atmospheric Chemistry and Physics Discussions

3.4.1 High-Arctic Sites

The high-Arctic sites of Eureka, Ny-Ålesund and Thule illustrate strong summertime enhancements of CO and HCN as seen in Figures 2 and 3, with a moderate enhancement of C_2H_6 shown in Figure 4. These enhancements have a maximum in July and August and from Figure 12, it is observed that the enhancements are largely due to the influence of BONA and BOAS wildfires. Wildfires in temperate regions (TENA and CEAS) are a small contribution to the CO tropospheric column (<5%) but do not contribute to the detected episodic enhancements. A moderate contribution to CO from CEAS and SEAS is observed, but these are not a source of anomalous enhancements.

Similar contributions are observed for BONA and BOAS among the high-Arctic sites, with a stronger influence from BONA to Eureka and Thule resulting in episodic enhancements of CO contributing greater than 40% to the CO tropospheric column. The strong influence of these sources is the result of the proximity of the high-Arctic sites to these source regions, as well as the efficient summertime isentropic transport (Stohl, 2006). As a result, the direct influence of wildfire plumes at the high-Arctic sites is observed in the FTIR time series, where the effects of plume dilution are minimal.

Furthermore, an early onset in April of the BOAS contribution is observed and is likely the result of the contribution from Siberian wildfires. Siberian wildfires are associated with low-level injected emissions, mainly within the planetary boundary layer and lower free troposphere (Val Martin et al., 2018). The low-level injection of these emissions and the high latitudes of the sources favour efficient transport to the Arctic (Stohl, 2006). In contrast, the Asian sources, CEAS and SEAS, show minor contributions to the CO tropospheric columns at the high-Arctic sites. Transport of these emissions to the Arctic are limited due to the higher potential temperature of these regions in the summertime, preventing isentropic transport to the Arctic (Klonecki, 2003; Stohl, 2006).

3.4.2 Arctic Sites

For the high-latitude European sites Kiruna and St. Petersburg, smaller contributions to CO from BONA and BOAS sources are observed, with peak contributions ranging from approximately 5 to 44% for BONA and 12 to 37% for BOAS, with slightly smaller contributions at Kiruna. The smaller contributions from these sites in comparison to the high-Arctic sites is partly due to the greater distances from the wildfire sources. The transport of emissions to these sites is a result of long-range westerly transport that generally exceeds 10 days (Damoah et al., 2004). Because of the long travel times, the plume is often diluted, and therefore, does not generally lead to the episodic enhancements observed at the high-Arctic sites. In contrast, Poker Flat is predominantly influenced by Alaskan wildfires, with contributions to the CO tropospheric column exceeding 50% in many cases. Similarly, the proximity of Poker Flat to BOAS sources makes BOAS a significant contributor to episodic CO enhancements, comparable to the local BONA source.

Similar to the high-Arctic sites, contributions from TENA, CEAS and SEAS to the Arctic sites are minimal and do not contribute to the episodic enhancements of CO, HCN and C_2H_6 detected in the FTIR time series. However, Poker Flat and St. Petersburg generally exhibit greater contributions from CEAS. For Poker Flat, this is the result of Asian outflow transporting emissions from Asian over the Atlantic to Alaska. For St. Petersburg, the proximity to the CEAS sources makes it susceptible

https://doi.org/10.5194/acp-2019-881
Preprint. Discussion started: 18 November 2019


Atmospheric Chemistry and Physics Discussions

to this source. Particularly evident is the large enhancement in July and August of 2010 due to wildfires in the Moscow region (Konovalov et al., 2011; Witte et al., 2011; Yurganov et al., 2011) although not detected in the FTIR time series as there were no measurements during that period.

3.4.3 Alpine Sites

The alpine sites, Zugspitze and Jungfraujoch shown in Figure 14, differ the most from the other sites considered in this study as a result of their high altitude. It is seen that Zugspitze and Jungfraujoch are most strongly influenced by BOAS, with a mean seasonal maximum contribution of approximately 14% at both sites. The contribution of BOAS emissions to the enhanced columns at Zugspitze and Jungfraujoch are due to hemispheric-scale transport (Damoah et al., 2004), leading to a perturbation to background concentrations of each species. As a result, the enhancements detected in the FTIR time series or GEOS-Chem do not result in the large, episodic enhancements observed at the high-Arctic sites. The contributions from trans-Atlantic transport of BONA emissions, however, exhibit these anomalous enhancements on occasion. Particularly evident are the BONA wildfires of 2013-2015 and 2018. Emissions from boreal Canadian wildfires may be injected into the free troposphere (Val Martin et al., 2018) and in some cases the lower stratosphere (Fromm et al., 2000; Khaykin et al., 2018; Peterson et al., 2018) which may enable the efficient transport of the plume over inter-continental scales (Heilman et al., 2014).

SEAS emissions are a larger contributor to CO enhancements for Zugspitze and Jungfraujoch than for the Arctic or high-Arctic sites. However, such enhancements are not observed in the FTIR time series as the contribution from SEAS is small in comparison to Asian anthropogenic sources as illustrated in Figure 11. Transport of Asian biomass burning CO emissions to Europe had been identified in the springtime by Petetin et al. (2018) and attributed to uplifting of emissions into the free troposphere and efficient transport of the westerlies (Bey et al., 2001a). In all cases, Zugspitze and Jungfraujoch are most susceptible to emissions that reach the free troposphere where long-range transport is favoured (Petetin et al., 2018).

3.4.4 Mid-latitude Sites

Anomalous enhancements in the Rikubetsu time series are dominated by the outflow of BOAS emissions that begin in early springtime and persist throughout the summer and autumn. Episodic BOAS enhancements are observed annually, with contributions that generally exceed 20% and are larger than 50% in many years. The greatest enhancement from BOAS was observed in 2003 as result of the exceptional emissions from Siberia wildfires (Jaffe et al., 2004; Ikeda and Tanimoto, 2015). Although the contribution from BOAS at Rikubetsu is highly variable between years, anomalous enhancements are observed annually in the GEOS-Chem time series, while detection of events in the FTIR time series is limited by the temporal sampling of the FTIR instrument. CEAS and SEAS have moderate contributions ($\sim$10%) to the CO tropospheric column at Rikubetsu in the spring and fall although the influence of these sources are often masked by the greater BOAS emissions during these periods. Other biomass burning sources have minimal contributions and Asian anthropogenic sources are dominant throughout the year as shown in Figure 11.

Toronto is most strongly influenced by wildfires of BONA, with detected events in the FTIR time series including 2014 from the Northwest Territories wildfires (Lutsch et al., 2016; Kochtubajda et al., 2019), 2015 from wildfires in Saskatchewan

https://doi.org/10.5194/acp-2019-881
Preprint. Discussion started: 18 November 2019


Atmospheric Chemistry and Physics Discussions

(Dreessen et al., 2016) and the 2017 British Columbia wildfires (Peterson et al., 2018). Although it is in close proximity to TENA sources, mainly from the Western and Southern United States, Toronto is minimally influenced by TENA as the magnitude of these emissions is much smaller than for BONA. Background contributions from CEAS and SEAS are also observed in the springtime although the contribution from Asian anthropogenic sources is dominant. BOAS is also a significant contribution to CO at Toronto in the summertime, but does not generally result in anomalous enhancements as a result of the longer transport times from this region. The 2018 enhancements were attributed to BOAS, while in June 2012, enhancements were present in the FTIR time series and appear to occur simultaneously with the large BOAS contribution (>30%). Minor contributions (<5%) from CEAS are observed in the springtime and autumn, while a moderate influence from SEAS of ∼10% is observed in the spring.

3.5 GEOS-Chem to FTIR CO Comparison

The GEOS-Chem CO partial column profiles are smoothed by the normalized FTIR CO total column averaging kernel following Rodgers and Connor (2003):

$$\hat{x}_m = x_a + \mathbf{a}^T (\mathbf{x}_m - \mathbf{x}_a), \tag{9}$$

where $\hat{x}_m$ is the smoothed model total column, x_a is the FTIR a priori total column, $\mathbf{x}_m$ is the model partial column profile, $\mathbf{a}$ is the FTIR total column averaging kernel, and $\mathbf{x}_a$ is the FTIR a priori partial column profile. Although the smoothing has a minor influence on the smoothed partial column (∼1%) it is performed here to mitigate any biases as a result of the a priori profile. The GEOS-Chem CO profiles, FTIR CO profiles and total column averaging kernels are daily averaged and the daily averaged GEOS-Chem profiles are subsequently smoothed. Correlations of the smoothed GEOS-Chem and FTIR CO tropospheric partial columns are shown in Figure 16.

For all sites, moderate to strong linear correlations are observed with correlation coefficients (r) ranging from a minimum of 0.66 for Toronto to a maximum of 0.89 at Thule. The slope of the linear regression is indicative of the GEOS-Chem bias relative to the FTIR measurements, with a slope greater than 1.0 representing a high-bias and a slope less than 1.0 representative of a low-bias. For all sites, GEOS-Chem has a low bias as seen in Figure 16. The slopes range from a minimum of 0.49 at Jungfraujoch to a maximum of 0.84 at both St. Petersburg and Rikubetsu.

The underestimation of GEOS-Chem CO is common amongst global CTMs as a result of errors in emissions, transport, and biases in the OH concentrations (Shindell et al., 2006). It is likely that the consistent underestimation of GEOS-Chem CO at all sites is partly due to a high bias of OH (Muller et al., 2018). Seasonal variability of the GEOS-Chem bias is observed as shown in Figure 17. The consistent underestimation of GEOS-Chem at Zugspitze and Jungfraujoch (as shown in Figure 17) may be the result of excessive stratosphere-to-troposphere exchange (Fischer et al., 2000; Hoor et al., 2002; Pan et al., 2004) contributed by the coarse model resolution, resulting in a low bias of CO in the upper troposphere. A similar underestimation of GEOS-Chem CO in a full-chemistry simulation in comparison to Jungfraujoch FTIR measurements was observed by Té et al. (2016). The high altitude of Zugspitze and Jungfraujoch makes these sites more susceptible to this bias in comparison to the

https://doi.org/10.5194/acp-2019-881
Preprint. Discussion started: 18 November 2019

Atmospheric Chemistry and Physics Discussions

lower altitude sites (Ordóñez et al., 2007). The underestimation at Toronto, and the lower correlation (0.66) than all other sites is possibly the result of the temporal and spatial variability of CO being not well captured due to the coarse model resolution ($2^\circ \times 2.5^\circ$).

Seasonal variability of the GEOS-Chem minus FTIR relative difference is also observed as shown in Figure 17 and tabulated in Table 6. The representation of the seasonal variability of transport at mid-latitudes and errors in the seasonality are likely to be contributing factors to the variability of the GEOS-Chem minus FTIR CO difference. However, biomass burning emissions are also seasonally dependent and underestimation of GEOS-Chem CO may be partially reflective of an underestimation of GFAS emissions. Particularly evident is the greater underestimation of GEOS-Chem at Rikubetsu in the summer months, during the boreal wildfire season. Eureka and Thule exhibit a greater underestimation of GEOS-Chem in July and August when the boreal wildfire influence is greatest as shown in Figure 12. A similar decrease in the GEOS-Chem minus FTIR relative difference is also observed at Kiruna, Poker Flat, St. Petersburg and Toronto. These differences could be indicative of the unresolved plume transport in the model as a result of its coarse vertical resolution (Rastigejev et al., 2010; Eastham and Jacob, 2017). Additionally, the summertime low CO bias in GEOS-Chem may also be contributed by an underestimation of the secondary production of CO from biogenic emissions of NMVOCs.

4 Conclusions

Boreal wildfires of North America (BONA) and Asia (BOAS) were found to be the greatest contributors to episodic CO enhancements at ten Northern hemisphere FTIR sites: Eureka, Ny-Ålesund, Thule, Kiruna, Poker Flat, St. Petersburg, Zugspitze, Jungfraujoch, Toronto and Rikubetsu. Wildfire pollution events were identified by detection of enhancements of CO in the FTIR time series. With the exception of Ny-Ålesund, Poker Flat and Rikubetsu, detected CO enhancements were correlated with coincident measurements of HCN and C_2H_6 to determine their enhancement ratios, providing evidence for the detection of wildfire pollution events. The GEOS-Chem tagged CO simulation allowed for source attribution of the detected events and for the source contribution to CO at each site to be evaluated.

The greatest numbers of FTIR enhancements were observed at Eureka (19) and Thule (17) due to their proximity to BONA and BOAS, with both sources contributing to greater than 40% of the CO tropospheric partial column in many cases. A similar influence of BONA and BOAS wildfires was observed at Ny-Ålesund, but the sparsity of the CO measurements limited detection of events in the FTIR time series. Furthermore, the lack of coincident measurement of HCN and C_2H_6 did not allow for enhancement ratios to be calculated for Ny-Ålesund.

Kiruna was also strongly influenced by the trans-Atlantic transport of BONA emissions and hemispheric transport of BOAS emissions, which may contribute ~5-40% of the CO tropospheric partial column during the summer months from June though September of each year. A similar contribution was observed at St. Petersburg, albeit lower in magnitude. The sparse measurements of CO, HCN and C_2H_6 at Poker Flat limited detection of events in the FTIR time series. However, the GEOS-Chem tagged CO simulation illustrated the strong influence of both BONA and BOAS sources at Poker Flat, which in several years exceeded 60% of the CO tropospheric column.

https://doi.org/10.5194/acp-2019-881
Preprint. Discussion started: 18 November 2019


Atmospheric Chemistry and Physics Discussions

The Alpine sites, Zugspitze and Jungfraujoch, are isolated from major biomass burning sources, but on occasion are subject to the transport of both BONA and BOAS emissions which were detected in the FTIR time series at both sites. However, these emissions are generally a small contribution to the tropospheric CO partial column (∼10%). Toronto was mainly influenced by North American wildfires of BONA contributing ∼10-20% of the CO column. Asian anthropogenic sources strongly influence the CO background at Rikubetsu, which was also considerably influenced by BOAS wildfires.

The results of this study show the Northern Hemispheric influence of boreal wildfire emissions, which were detected using FTIR measurements of CO and the coincident measurements of HCN and C_2H_6. The inter-annual variability of boreal wildfire emissions observed in the GEOS-Chem tagged CO simulation was also observed in the detected FTIR enhancements when measurements were available. The detected FTIR enhancements from 2013-2018 were in most cases attributed to BONA, consistent with the increase in the BONA contribution to CO during this period as observed in the GEOS-Chem time series.

Code and data availability. The FTIR data are available from the NDACC data repository at ftp://ftp.cpc.ncep.noaa.gov/ndacc/. The GEOS data used in this study have been provided by the Global Modeling and Assimilation Office (GMAO) at NASA Goddard Space Flight Center.The GEOS-Chem model code used is available here: http://dx.doi.org/10.5281/zenodo.2249246 (The International GEOS-Chem User Community, 2018). The AEORONET data used are available here: https://aeronet.gsfc.nasa.gov/cgi-bin/draw_map_display_aod_v3. Any additional data may be obtained from Erik Lutsch (elutsch@physics.utoronto.ca)

Author contributions. This study was designed EL, KS and DBAJ. TB, SC, JWH, FH, YK, EM, MM, IM, TN, JN, IO, MO, AVP, RS and TW contributed to the FTIR measurements used. JAF contributed to the updated GEOS-Chem tagged CO simulation that was used. The analysis was performed by the EL. The paper was prepared by EL with contributions from all authors.

Competing interests. The authors declare they have no competing interests.

Acknowledgements. Bruker FTIR measurements were made at PEARL by the Canadian Network for the Detection of Atmospheric Composition Change (CANDAC), which has been supported by the Atlantic Innovation Fund/Nova Scotia Research Innovation Trust, Canada Foundation for Innovation, Canadian Foundation for Climate and Atmospheric Sciences, Canadian Space Agency (CSA), Environment and Climate Change Canada (ECCC), Government of Canada International Polar Year funding, Natural Sciences and Engineering Research Council (NSERC), Northern Scientific Training Program, Ontario Innovation Trust, Polar Continental Shelf Program, and Ontario Research Fund. EL was partially supported by the NSERC CREATE Training Program in Arctic Atmospheric Science and the Probing Atmosphere in the High Arctic (PAHA) project. We thank CANDAC/PEARL/PAHA PI James Drummond, Canadian Arctic ACE/OSIRIS Validation Campaign PI Kaley Walker, PEARL Site Manager Pierre Fogal, CANDAC Data Manager Yan Tsehtik, the CANDAC operators, and the staff at ECCCs Eureka Weather Station for their contributions to data acquisition, and for logistical and on-site support.

https://doi.org/10.5194/acp-2019-881
Preprint. Discussion started: 18 November 2019

Atmospheric Chemistry and Physics Discussions

The National Center for Atmospheric Research (NCAR) is sponsored by the U.S. National Science Foundation (NSF). The NCAR FTIR observation program at Thule, Greenland is supported under contract by the National Aeronautics and Space Administration (NASA). The Thule work is also supported by the NSF Office of Polar Programs (OPP). We wish to thank the Danish Meteorological Institute for support at the Thule site. KIT, IMK-ASF would like to thank Uwe Raffalski and Peter Voelger from the Swedish Institute of Space Physics (IRF) for their continuing support of the NDACC-FTIR site Kiruna. St. Petersburg State University was supported by the RFBR project #18-05-00011. MP gratefully acknowledges funding from the Deutsche Forschungsgemeinschaft (DFG, German Research Foundation; project number 268020496, TRR 172) within the Transregional Collaborative Research Center ArctiC Amplification: Climate Relevant Atmospheric and SurfaCe Processes, and Feedback Mechanisms (AC)3" in subproject E02. St. Petersburg FTIR measurements were carried out by the instrumentation of the Geomodel resource center of SPbU. JAF acknowledges funding from the University of Wollongong and the Australian Research Council (DP160101598) as well as computational resources provided at the NCI National Facility systems at the Australian National University through the National Computational Merit Allocation Scheme supported by the Australian Government. Operation at the Rikubetsu site is supported in part by the GOSAT series project.

The authors acknowledge the use of AERONET data and thank Norm O'Neill, Ihab Abboud Vitali Fioletov, Brent Holben, Piotr Sobolewski, Piotr Glowacki, Grzegorz Karasinski, Victoria E. Cachorro Revilla, Sandra Blindheim, John R. Vande Castle, Margit Aun, Natalia Kouremeti, Itaru Sano and their staff for establishing and maintaining the 9 sites used in this investigation. The authors acknowledge the use of the GFASv1.2 emissions inventory, which contains modified Copernicus Atmosphere Monitoring Service information (2019). We also acknowledge Mathew J. Evans, Eleanor Morris and Killian Murphy for providing the GFASv1.2 netCDF files. The GEOS data used in this study have been provided by the Global Modeling and Assimilation Office (GMAO) at NASA Goddard Space Flight Center.

https://doi.org/10.5194/acp-2019-881
Preprint. Discussion started: 18 November 2019

Atmospheric Chemistry and Physics Discussions

References

Akagi, S. K., Yokelson, R. J., Wiedinmyer, C., Alvarado, M. J., Reid, J. S., Karl, T., Crounse, J. D., and Wennberg, P. O.: Emission factors for open and domestic biomass burning for use in atmospheric models, Atmospheric Chemistry and Physics, 11, 4039–4072, https://doi.org/10.5194/acp-11-4039-2011, 2011.

Amiro, B. D., Cantin, A., Flannigan, and de Groot, W. J.: Future emissions from Canadian boreal forest fires, Canadian Journal of Forest Research, 39, 383–395, https://doi.org/10.1139/X08-154, 2009.

Andreae, M. O.: Emission of trace gases and aerosols from biomass burning - An updated assessment, Atmospheric Chemistry and Physics, 19, 8523–8546, https://doi.org/10.5194/acp-19-8523-2019, 2019.

Andreae, M. O. and Merlet, P.: Emission of trace gases and aerosols from biomass burning, Global Biogeochemical Cycles, 15, 955–966, https://doi.org/10.1029/2000GB001382, 2001.

Arola, A., Lindfors, A., Natunen, A., and Lehtinen, K. E. J.: A case study on biomass burning aerosols: effects on aerosol optical properties and surface radiation levels, Atmospheric Chemistry and Physics, 7, 4257–4266, https://doi.org/10.5194/acp-7-4257-2007, 2007.

Barret, B., Mazière, M. D., and Mahieu, E.: Ground-based FTIR measurements of CO from the Jungfraujoch: characterisation and comparison with in situ surface and MOPITT data, Atmospheric Chemistry and Physics, 3, 2217–2223, https://doi.org/10.5194/acp-3-2217-2003, 2003.

Batchelor, R. L., Strong, K., Lindenmaier, R., Mittermeier, R. L., Fast, H., Drummond, J. R., and Fogal, P. F.: A new Bruker IFS 125HR FTIR spectrometer for the Polar Environment Atmospheric Research Laboratory at Eureka, Nunavut, Canada: measurements and comparison with the existing Bomem DA8 spectrometer, Journal of Atmospheric and Oceanic Technology, 26, 1328–1340, https://doi.org/10.1175/2009JTECHA1215.1, 2009.

Baum, M. M., Moss, J. A., Pastel, S. H., and Poskrebyshev, G. A.: Hydrogen cyanide exhaust emissions from in-use motor vehicles, Environmental Science & Technology, 41, 857–862, https://doi.org/10.1021/es061402v, 2007.

Bey, I., Jacob, D. J., Logan, J. A., and Yantosca, R. M.: Asian chemical outflow to the Pacific in spring: Origins, pathways, and budgets, Journal of Geophysical Research: Atmospheres, 106, 23 097–23 113, https://doi.org/10.1029/2001JD000806, 2001a.

Bey, I., Jacob, D. J., Yantosca, R. M., Logan, J. A., Field, B. D., Fiore, A. M., Li, Q., Liu, H. Y., Mickley, L. J., and Schultz, M. G.: Global modeling of tropospheric chemistry with assimilated meteorology: Model description and evaluation, Journal of Geophysical Research: Atmospheres, 106, 23 073–23 095, https://doi.org/10.1029/2001JD000807, 2001b.

Blumenstock, T., Hase, F., Kramer, I., Mikuteit, S., Fischer, H., Goutail, F., and Raffalski, U.: Winter to winter variability of chlorine activation and ozone loss as observed by ground-based FTIR measurements at Kiruna since winter 1993/94, International Journal of Remote Sensing, 30, 4055–4064, https://doi.org/10.1080/01431160902821916, 2009.

Blumenstock, T. H., Fisher, H., Friedle, A., Hase, F., and Thomas, P.: Column Amounts of $ClONO_2$, HCl, HNO_3, and HF from Ground-Based FTIR Measurements Made Near Kiruna, Sweden, in Late Winter 1994, Journal of Atmospheric Chemistry, 26, 311–321, https://doi.org/10.1023/A:1005728713762, 1997.

Bond, T. C. and Sun, H.: Can reducing black carbon emissions counteract global warming?, Environmental Science & Technology, 39, 5921–5926, 2005.

Boulanger, Y., Gauthier, S., and Burton, P. J.: A refinement of models projecting future Canadian fire regimes using homogeneous fire regime zones, Canadian Fournal of Forest Research, 44, 365–376, https://doi.org/10.1139/cjfr-2013-0372, 2014.

https://doi.org/10.5194/acp-2019-881
Preprint. Discussion started: 18 November 2019

Atmospheric Chemistry and Physics Discussions

Cicerone, R. J. and Zellner, R.: The atmospheric chemistry of hydrogen cyanide (HCN), Journal of Geophysical Research: Atmospheres, 88, 10 689–10 696, https://doi.org/10.1029/JC088iC15p10689, 1983.

Conard, S. G. and Ivanova, G. A.: Wildfire in Russian Boreal Forests - Potential Impacts of Fire Regime Characteristics on Emissions and Global Carbon Balance Estimates, Environmental Pollution, 98, 305–313, https://doi.org/10.1016/S0269-7491(97)00140-1, 1997.

Crippa, M., Janssens-Maenhout, G., Dentener, F., Guizzardi, D., Sindelarova, K., Muntean, M., Van Dingenen, R., and Granier, C.: Forty years of improvements in European air quality: regional policy-industry interactions with global impacts, Atmospheric Chemistry and Physics, 16, 3825–3841, https://doi.org/10.5194/acp-16-3825-2016, 2016.

Dammers, E., Vigouroux, C., Palm, M., Mahieu, E., Warneke, T., Smale, D., Langerock, B., Franco, B., Van Damme, M., Schaap, M., Notholt, J., and Erisman, J. W.: Retrieval of ammonia from ground-based FTIR solar spectra, Atmospheric Chemistry and Physics, 15, 12 789–12 803, https://doi.org/10.5194/acp-15-12789-2015, 2015.

Damoah, R., Spichtinger, N., Forster, C., James, P., Mattis, I., Wandinger, U., Beirle, S., Wagner, T., and Stohl, A.: Around the world in 17 days - Hemispheric-scale transport of forest fire smoke from Russia in May 2003, Atmospheric Chemistry and Physics, 4, 1311–1321, https://doi.org/10.5194/acp-4-1311-2004, 2004.

De Mazière, M., Thompson, A. M., Kurylo, M. J., Wild, J. D., Bernhard, G., Blumenstock, T., Braathen, G. O., Hannigan, J. W., Lambert, J.-C., Leblanc, T., McGee, T. J., Nedoluha, G., Petropavlovskikh, I., Seckmeyer, G., Simon, P. C., Steinbrecht, W., and Strahan, S. E.: The Network for the Detection of Atmospheric Composition Change (NDACC): History, status and perspectives, Atmospheric Chemistry and Physics, 18, 4935–4964, https://doi.org/10.5194/acp-18-4935-2018, 2018.

Dreessen, J., Sullivan, J., and Delgado, R.: Observations and impacts of transported Canadian wildfire smoke on ozone and aerosol air quality in the Maryland region on June 9-12, 2015, Journal of the Air & Waste Management Association, 66, 842–862, https://doi.org/10.1080/10962247.2016.1161674, 2016.

Eastham, S. D. and Jacob, D. J.: Limits on the ability of global Eulerian models to resolve intercontinental transport of chemical plumes, Atmospheric Chemistry and Physics, 17, 2543–2553, https://doi.org/10.5194/acp-17-2543-2017, 2017.

Eck, T. F., Holben, B. N., Reid, J. S., Sinyuk, A., Hyer, E. J., O'Neill, N. T., Shaw, G. E., Vande Castle, J. R., Chapin, F. S., Dubovik, O., Smirnov, A., Vermote, E., Schafer, J. S., Giles, D., Slutsker, I., Sorokine, M., and Newcomb, W. W.: Optical properties of boreal region biomass burning aerosols in central Alaska and seasonal variation of aerosol optical depth at an Arctic coastal site, Journal of Geophysical Research: Atmospheres, 114, 722–4740, https://doi.org/10.1029/2008JD010870, 2009.

Evangeliou, N., Balkanski, Y., Hao, W. M., Petkov, A., Silverstein, R. P., Corley, R., Nordgren, B. L., Urbanski, S. P., Eckhardt, S., Stohl, A., and Others: Wildfires in northern Eurasia affect the budget of black carbon in the Arctic - A 12-year retrospective synopsis (2002-2013), Atmospheric Chemistry and Physics, 16, 7587–7604, 2016.

Fischer, H., Wienhold, F. G., Hoor, P., Bujok, O., Schiller, C., Siegmund, P., Ambaum, M., Scheeren, H. A., and Lelieveld, J.: Tracer correlations in the northern high latitude lowermost stratosphere: Influence of cross-tropopause mass exchange, Geophysical Research Letters, 27, 97–100, https://doi.org/10.1029/1999GL010879, 2000.

Fisher, J. A., Jacob, D. J., Purdy, M. T., Kopacz, M., Sager, P. L., Carouge, C., Holmes, C. D., Yantosca, R. M., Batchelor, R. L., Strong, K., Diskin, G. S., Fuelberg, H. E., Holloway, J. S., Hyer, E. J., McMillan, W. W., Warner, J., Streets, D. G., Zhang, Q., Wang, Y., and Wu, S.: Source attribution and interannual variability of Arctic pollution in spring constrained by aircraft (ARCTAS, ARCPAC) and satellite (AIRS) observations of carbon monoxide, Atmospheric Chemistry and Physics, 10, 977–996, https://doi.org/10.5194/acp-10-977-2010, 2010.

https://doi.org/10.5194/acp-2019-881
Preprint. Discussion started: 18 November 2019

Atmospheric Chemistry and Physics Discussions

Fisher, J. A., Murray, L., Jones, D. B. A., and Deutscher, N. M.: Improved method for linear carbon monoxide simulation and source attribution in atmospheric chemistry models illustrated using GEOS-Chem v9, Geophysical Model Development, 10, 4129–4144, https://doi.org/10.5194/gmd-10-4129-2017, 2017.

Flanner, M. G.: Arctic climate sensitivity to local black carbon, Journal of Geophysical Research: Atmospheres, 118, 1840–1851, 2013.

Flannigan, M. D., Krawchuk, M. A., de Groot, W. J., Mike Wotton, B., and Gowman, L. M.: Implications of changing climate for global wildland fire, International Journal of Wildland Fire, 18, 483–507, https://doi.org/10.1071/WF08187, 2009.

Franco, B., Bader, W., Toon, G. C., Bray, C., Perrin, A., Fischer, E. V., Sudo, K., Boone, C. D., Bovy, B., Lejeune, B., Servais, C., and Mahieu, E.: Retrieval of ethane from ground-based FTIR solar spectra using improved spectroscopy: Recent burden increase above Jungfraujoch, Journal of Quantitative Spectroscopy & Radiative Transfer, 160, 36–49, https://doi.org/10.1016/j.jqsrt.2015.03.017, 2015.

Freitas, S. R., Longo, K. M., Chatfield, R., Latham, D., Silva Dias, M. A. F., Andreae, M. O., Prins, E., Santos, J. C., Gielow, R., and Carvalho, Jr, J. A.: Including the sub-grid scale plume rise of vegetation fires in low resolution atmospheric transport models, Atmospheric Chemistry and Physics, 7, 3385–3398, 2007.

Fromm, M., Alfred, J., Hoppel, K., Hornstein, J., Bevilacqua, R., Shettle, E., Servranckx, R., Li, Z., and Stocks, B.: Observations of boreal forest fire smoke in the stratosphere by POAM III, SAGE II, and lidar in 1998, Geophysical Research Letters, 27, 1407–1410, https://doi.org/10.1029/1999GL011200, 2000.

Gelaro, R., McCarty, W., Suárez, M. J., Todling, R., Molod, A., Takacs, L., Randles, C. A., Darmenov, A., Bosilovich, M. G., Reichle, R., Wargan, K., Coy, L., Cullather, R., Draper, C., Akella, S., Buchard, V., Conaty, A., da Silva, A. M., Gu, W., Kim, G.-K., Koster, R., Lucchesi, R., Merkova, D., Nielsen, J. E., Partyka, G., Pawson, S., Putman, W., Rienecker, M., Schubert, S. D., Sienkiewicz, M., and Zhao, B.: The Modern-Era Retrospective Analysis for Research and Applications, Version 2 (MERRA-2), Journal of Climate, 30, 5419–5454, https://doi.org/10.1175/JCLI-D-16-0758.1, 2017.

Giglio, L., Randerson, J. T., and van der Werf, G. R.: Analysis of daily, monthly, and annual burned area using the fourth-generation global fire emissions database (GFED4), Journal of Geophysical Research: Biogeosciences, 118, 317–328, https://doi.org/10.1002/jgrg.20042, 2013.

Giles, D. M., Sinyuk, A., Sorokin, M. G., Schafer, J. S., Smirnov, A., Slutsker, I., Eck, T. F., Holben, B. N., Lewis, J. R., Campbell, J. R., Welton, E. J., Korkin, S. V., and Lyapustin, A. I.: Advancements in the Aerosol Robotic Network (AERONET) Version 3 database - automated near-real-time quality control algorithm with improved cloud screening for Sun photometer aerosol optical depth (AOD) measurements, Atmospheric Measurement Techniques, 12, 169–209, https://doi.org/10.5194/amt-12-169-2019, 2019.

Giuseppe, F. D., Rémy, S., Pappenberger, F., and Wetterhall, F.: Using the Fire Weather Index (FWI) to improve the estimation of fire emissions from fire radiative power (FRP) observations, Atmospheric Chemistry and Physics, 18, 5359–5370, https://doi.org/10.5194/acp-18-5359-2018, 2018.

Goode, J. G., Yokelson, R. J., Susott, R. A., and Ward, D. E.: Trace gas emissions from laboratory biomass fires measured by open-path Fourier transform infrared spectroscopy: Fires in grass and surface fuels, Journal of Geophysical Research: Atmospheres, 104, 21 237–21 245, https://doi.org/10.1029/1999JD900360, 1999.

Goode, J. G., Yokelson, R. J., Ward, D. E., Susott, R. A., Babbitt, R. E., Davies, M. A., and Hao, W. M.: Measurements of excess O_3, CO_2, CO, CH_4, C_2H_4, C_2H_2, HCN, NO, NH_3, HCOOH, CH_3COOH, HCHO, and CH_3OH in 1997 Alaskan biomass burning plumes by airborne Fourier transform infrared spectroscopy (AFTIR), Journal of Geophysical Research: Atmospheres, 105, 22 147–22 166, https://doi.org/10.1029/2000JD900287, 2000.

https://doi.org/10.5194/acp-2019-881
Preprint. Discussion started: 18 November 2019

Griffin, D., Walker, K. A., Franklin, J. E., Parrington, M., Whaley, C., Hopper, J., Drummond, J. R., Palmer, P. I., Strong, K., Duck, T. J., Abboud, I., Bernath, P. F., Clerbaux, C., Coheur, P.-F., Curry, K. R., Dan, L., Hyer, E., Kliever, J., Lesins, G., Maurice, M., Saha, A., Tereszchuk, K., and Weaver, D.: Investigation of CO, C_2H_6 and aerosols in a boreal fire plume over eastern Canada during BORTAS 2011 using ground- and satellite-based observations and model simulations, Atmospheric Chemistry and Physics, 13, 10 227–10 241, https://doi.org/10.5194/acp-13-10227-2013, 2013.

Gubler, S., Gruber, S., and Purves, R. S.: Uncertainties of parameterized surface downward clear-sky shortwave and all-sky longwave radiation, Atmospheric Chemistry and Physics, 12, 5077–5098, https://doi.org/10.5194/acp-12-5077-2012, 2012.

Guenther, A., Geron, C., Pierce, T., Lamb, B., Harley, P., and Fall, R.: Natural emissions of non-methane volatile organic compounds, carbon monoxide, and oxides of nitrogen from North America, Atmospheric Environment, 34, 2205–2230, https://doi.org/10.1016/S1352-2310(99)00465-3, 2000.

Guenther, A. B., Jiang, X., Heald, C. L., Sakulyanontvittaya, T., Duhl, T., Emmons, L. K., and Wang, X.: The Model of Emissions of Gases and Aerosols from Nature version 2.1 (MEGAN2.1): An extended and updated framework for modeling biogenic emissions, Geoscientific Model Development, 5, 1471–1492, https://doi.org/10.5194/gmd-5-1471-2012, 2012.

Hannigan, J. W., Coffey, M. T., and Goldman, A.: Semiautonomous FTS Observation System for Remote Sensing of Stratospheric and Tropospheric Gases, Journal of Atmospheric and Oceanic Technology, 26, 1814–1828, https://doi.org/10.1175/2009JTECHA1230.1, 2009.

Hase, F., Hannigan, J. W., Coffey, M. T., Goldman, A., Höpfner, M., Jones, N. B., Rinsland, C. P., and Wood, S. W.: Intercomparison of retrieval codes used for the analysis of high-resolution, ground-based FTIR measurements, Journal of Quantitative Spectroscopy & Radiative Transfer, 87, 25–52, https://doi.org/10.1016/j.jqsrt.2003.12.008, 2004.

Heilman, W. E., Liu, Y., Urbanski, S., Kovalev, V., and Mickler, R.: Wildland fire emissions, carbon, and climate: Plume rise, atmospheric transport, and chemistry processes, Forest Ecology and Management, 317, 70–79, https://doi.org/10.1016/j.foreco.2013.02.001, 2014.

Henne, S., Brunner, D., Folini, D., Solberg, S., Klausen, J., and Buchmann, B.: Assessment of parameters describing representativeness of air quality in-situ measurement sites, Atmospheric Chemistry and Physics, 10, 3561–3581, https://doi.org/10.5194/acp-10-3561-2010, 2010.

Holben, B. N., Eck, T. F., Slutsker, I., Tanré, D., Buis, J. P., Setzer, A., Vermote, E., Reagan, J. A., Kaufman, Y. J., Nakajima, T., Lavenu, F., Jankowiak, I., and Smirnov, A.: AERONET - A Federated Instrument Network and Data Archive for Aerosol Characterization, Remote Sensing of Environment, 66, 1–16, https://doi.org/10.1016/S0034-4257(98)00031-5, 1998.

Holloway, T., Levy, H., and Kasibhatla, P.: Global distribution of carbon monoxide, Journal of Geophysical Research: Atmospheres, 105, 12 123–12 147, https://doi.org/10.1029/1999JD901173, 2000.

Holtslag, A. A. M. and Boville, B. A.: Local Versus Nonlocal Boundary-Layer Diffusion in a Global Climate Model, Journal of Climate, 6, 1825–1842, https://doi.org/10.1175/1520-0442(1993)006<1825:LVNBLD>2.0.CO;2, 1993.

Honrath, R. E.: Regional and hemispheric impacts of anthropogenic and biomass burning emissions on summertime CO and O_3 in the North Atlantic lower free troposphere, Journal of Geophysical Research: Atmospheres, 109, https://doi.org/10.1029/2004JD005147, 2004.

Hoor, P., Fischer, H., Lange, L., Lelieveld, J., and Brunner, D.: Seasonal variations of a mixing layer in the lowermost stratosphere as identified by the CO-O_3 correlation from in situ measurements, Journal of Geophysical Research: Atmospheres, 107, ACL 1–1–ACL 1–11, https://doi.org/10.1029/2000JD000289, 2002.

Hu, Q., Goloub, P., Veselovskii, I., Bravo-Aranda, J.-A., Popovici, I. E., Podvin, T., Haeffelin, M., Lopatin, A., Dubovik, O., Pietras, C., Huang, X., Torres, B., and Chen, C.: Long-range-transported Canadian smoke plumes in the lower stratosphere over northern France, Atmospheric Chemistry and Physics, 19, 1173–1193, https://doi.org/10.5194/acp-19-1173-2019, 2019.

https://doi.org/10.5194/acp-2019-881
Preprint. Discussion started: 18 November 2019

Atmospheric Chemistry and Physics Discussions

Ikeda, K. and Tanimoto, H.: Exceedances of air quality standard level of PM2.5 in Japan caused by Siberian wildfires, Environmental Research Letters, 10, 105 001, https://doi.org/10.1088/1748-9326/10/10/105001, 2015.

Jaffe, D., Anderson, T., Covert, D., Kotchenruther, R., Trost, B., Danielson, J., Simpson, W., Berntsen, T., Karlsdottir, S., Blake, D., Harris, J., Carmichael, G., and Uno, I.: Transport of Asian air pollution to North America, Geophysical Research Letters, 26, 711–714, https://doi.org/10.1029/1999GL900100, 1999.

Jaffe, D., Bertschi, I., Jaeglé, L., Novelli, P., Reid, J. S., Tanimoto, H., Vingarzan, R., and Westphal, D. L.: Long-range transport of Siberian biomass burning emissions and impact on surface ozone in western North America, Geophysical Research Letters, 31, https://doi.org/10.1029/2004GL020093, 2004.

Jeong, J. I., Park, R. J., and Youn, D.: Effects of Siberian forest fires on air quality in East Asia during May 2003 and its climate implication, Atmospheric Environment, 42, 8910–8922, https://doi.org/10.1016/j.atmosenv.2008.08.037, 2008.

Kaiser, J. W., Heil, A., Andreae, M. O., Benedetti, A., Chubarova, N., Jones, L., Morcrette, J.-J., Razinger, M., Schultz, M. G., Suttie, M., and van der Werf, G. R.: Biomass burning emissions estimated with a global fire assimilation system based on observed fire radiative power, Biogeosciences, 9, 527–554, https://doi.org/10.5194/bg-9-527-2012, 2012.

Kasai, Y. J., Kagawa, A., Jones, N., Fujiwara, A., Seki, K., Murayama, Y., and Murcray, F.: Seasonal variations of CO and HCN in the troposphere measured by solar absorption spectroscopy over Poker Flat, Alaska, Geophysical Research Letters, 32, 1–4, https://doi.org/10.1029/2005GL022826, 2005a.

Kasai, Y. J., Koshiro, T., Endo, M., Jones, N. B., and Murayama, Y.: Ground-based measurement of strato–mesospheric CO by a FTIR spectrometer over Poker Flat, Alaska, Advances in Space Research, 35, 2024–2030, https://doi.org/10.1016/j.asr.2005.04.099, 2005b.

Khaykin, S. M., Godin-Beekmann, S., Hauchecorne, A., Pelon, J., Ravetta, F., and Keckhut, P.: Stratospheric Smoke With Unprecedentedly High Backscatter Observed by Lidars Above Southern France, Geophysical Research Letters, 45, 1639–1646, https://doi.org/10.1002/2017GL076763, 2018.

Kirchmeier-Young, M. C., Gillett, N. P., Zwiers, F. W., Cannon, A. J., and Anslow, F. S.: Attribution of the Influence of Human-Induced Climate Change on an Extreme Fire Season, Earth's Future, 7, 2–10, https://doi.org/10.1029/2018EF001050, 2019.

Klonecki, A.: Seasonal changes in the transport of pollutants into the Arctic troposphere-model study, Journal of Geophysical Research: Atmospheres, 108, 8367, https://doi.org/10.1029/2002JD002199, 2003.

Kochtubajda, B., Stewart, R. E., Flannigan, M. D., Bonsal, B. R., Cuell, C., and Mooney, C. J.: An Assessment of Surface and Atmospheric Conditions Associated with the Extreme 2014 Wildfire Season in Canada's Northwest Territories, Atmosphere-Ocean, 57, 73–90, https://doi.org/10.1080/07055900.2019.1576023, 2019.

Konovalov, I. B., Beekmann, M., Kuznetsova, I. N., Yurova, A., and Zvyagintsev, A. M.: Atmospheric impacts of the 2010 Russian wildfires: Integrating modelling and measurements of an extreme air pollution episode in the Moscow region, Atmospheric Chemistry and Physics, 11, 10 031–10 056, https://doi.org/10.5194/acp-11-10031-2011, 2011.

Kozlov, V. S., Yausheva, E. P., Terpugova, S. A., Panchenko, M. V., Chernov, D. G., and Shmargunov, V. P.: Optical–microphysical properties of smoke haze from Siberian forest fires in summer 2012, International Journal of Remote Sensing, 35, 5722–5741, https://doi.org/10.1080/01431161.2014.945010, 2014.

Krause, A., Kloster, S., Wilkenskjeld, S., and Paeth, H.: The sensitivity of global wildfires to simulated past, present, and future lightning frequency, Journal of Geophysical Research: Biogeosciences, 119, 312–322, https://doi.org/10.1002/2013JG002502, 2014.

Kurylo, M. J.: Network for the Detection of Stratospheric Change, https://doi.org/10.1117/12.46658, 1991.

Law, K. S. and Stohl, A.: Arctic air pollution: origins and impacts, Science, 315, 1537–1540, https://doi.org/10.1126/science.1137695, 2007.

https://doi.org/10.5194/acp-2019-881
Preprint. Discussion started: 18 November 2019

Atmospheric Chemistry and Physics Discussions

Lefer, B. L., Talbot, R. W., Harriss, R. H., Bradshaw, J. D., Sandholm, S. T., Olson, J. O., Sachse, G. W., Collins, J., Shipham, M. A., Blake, D. R., Klemm, K. I., Klemm, O., Gorzelska, K., and Barrick, J.: Enhancement of acidic gases in biomass burning impacted air masses over Canada, Journal of Geophysical Research: Atmospheres, 99, 1721–1737, https://doi.org/10.1029/93JD02091, 1994.

Levine, J. S.: 4.05 - Biomass Burning: The Cycling of Gases and Particulates from the Biosphere to the Atmosphere, in: Treatise on Geochemistry, edited by Holland, H. D. and Turekian, K. K., pp. 143–158, Pergamon, Oxford, https://doi.org/10.1016/B0-08-043751-6/04143-8, 2003.

Li, Q., Jacob, D. J., Bey, I., Yantosca, R. M., Zhao, Y., Kondo, Y., and Notholt, J.: Atmospheric hydrogen cyanide (HCN): Biomass burning source, ocean sink?, Geophysical Research Letters, 27, 357–360, https://doi.org/10.1029/1999GL010935, 2000.

Li, Q., Jacob, D. J., Yantosca, R. M., Heald, C. L., Singh, H. B., Koike, M., Zhao, Y., Sachse, G. W., and Streets, D. G.: A global three-dimensional model analysis of the atmospheric budgets of HCN and CH_3CN: Constraints from aircraft and ground measurements, Journal of Geophysical Research: Atmospheres, 108, 8827, https://doi.org/10.1029/2002JD003075, 2003.

Li, Q., Palmer, P. I., Pumphrey, H. C., Bernath, P., and Mahieu, E.: What drives the observed variability of HCN in the troposphere and lower stratosphere?, Atmospheric Chemistry and Physics, 9, 8531–8543, https://doi.org/10.5194/acp-9-8531-2009, 2009.

Logan, J. A., Prather, M. J., Wofsy, S. C., and McElroy, M. B.: Tropospheric chemistry: A global perspective, Journal of Geophysical Research: Oceans, 86, 7210–7254, https://doi.org/10.1029/JC086iC08p07210, 1981.

Lutsch, E., Dammers, E., Conway, S., and Strong, K.: Long-range transport of NH_3, CO, HCN, and C_2H_6 from the 2014 Canadian Wildfires, Geophysical Research Letters, 43, 8286–8297, https://doi.org/10.1002/2016GL070114, 2016.

Lutsch, E., Strong, K., Jones, D. B. A., Ortega, I., Hannigan, J. W., Dammers, E., Shephard, M. W., Morris, E., Murphy, K., Evans, M. J., Parrington, M., Whitburn, S., Van Damme, M., Clarisse, L., Coheur, P., Clerbaux, C., Croft, B., Martin, R. V., Pierce, J. R., and Fisher, J. A.: Unprecedented Atmospheric Ammonia Concentrations Detected in the High Arctic From the 2017 Canadian Wildfires, Journal of Geophysical Research: Atmospheres, 124, 8178–8202, https://doi.org/10.1029/2019JD030419, 2019.

Macias Fauria, M. and Johnson, E. A.: Large-scale climatic patterns control large lightning fire occurrence in Canada and Alaska forest regions, Journal of Geophysical Research: Biogeosciences, 111, 2006.

Macias Fauria, M. and Johnson, E. A.: Climate and wildfires in the North American boreal forest, Philosophical transactions of the Royal Society of London. Series B, Biological Sciences, 363, 2315–2327, https://doi.org/10.1098/rstb.2007.2202, 2008.

Mack, M. C., Bret-Harte, M. S., Hollingsworth, T. N., Jandt, R. R., Schuur, E. A. G., Shaver, G. R., and Verbyla, D. L.: Carbon loss from an unprecedented Arctic tundra wildfire, Nature, 475, 489–492, https://doi.org/10.1038/nature10283, 2011.

Mahieu, E., Zander, R., Delbouille, L., Demoulin, P., Roland, G., and Servais, C.: Observed trends in total vertical column abundances of atmospheric gases from IR solar spectra recorded at the Jungfraujoch, Journal of Atmospheric Chemistry, 28, 227–243, https://doi.org/10.1023/A:1005854926740, 1997.

Makar, P. A., Akingunola, A., Aherne, J., Cole, A. S., Aklilu, Y.-A., Zhang, J., Wong, I., Hayden, K., Li, S.-M., Kirk, J., Scott, K., Moran, M. D., Robichaud, A., Cathcart, H., Baratzedah, P., Pabla, B., Cheung, P., Zheng, Q., and Jeffries, D. S.: Estimates of exceedances of critical loads for acidifying deposition in Alberta and Saskatchewan, Atmospheric Chemistry and Physics, 18, 9897–9927, https://doi.org/10.5194/acp-18-9897-2018, 2018.

Makarova, M. V., Poberovskii, A. V., and Osipov, S. I.: Time variations of the total CO content in the atmosphere near St. Petersburg, Izvestiya, Atmospheric and Oceanic Physics, 47, 739–746, https://doi.org/10.1134/S0001433811060090, 2011.

https://doi.org/10.5194/acp-2019-881
Preprint. Discussion started: 18 November 2019

Atmospheric Chemistry and Physics Discussions

McConnell, J. R., Edwards, R., Kok, G. L., Flanner, M. G., Zender, C. S., Saltzman, E. S., Banta, J. R., Pasteris, D. R., Carter, M. M., and Kahl, J. D. W.: 20th-century industrial black carbon emissions altered Arctic climate forcing, Science, 317, 1381–1384, https://doi.org/10.1126/science.1144856, 2007.

Moussa, S. G., Leithead, A., Li, S.-M., Chan, T. W., Wentzell, J. J. B., Stroud, C., Zhang, J., Lee, P., Lu, G., Brook, J. R., Hayden, K., Narayan, J., and Liggio, J.: Emissions of hydrogen cyanide from on-road gasoline and diesel vehicles, Atmospheric Environment, 131, 185–195, https://doi.org/10.1016/j.atmosenv.2016.01.050, 2016.

Muller, J.-F., Stavrakou, T., Bauwens, M., George, M., Hurtmans, D., Coheur, P.-F., Clerbaux, C., and Sweeney, C.: Top-Down CO Emissions Based On IASI Observations and Hemispheric Constraints on OH Levels, Geophysical Research Letters, 45, 1621–1629, https://doi.org/10.1002/2017GL076697, 2018.

Notholt, J., Toon, G., Stordal, F., Solberg, S., Schmidbauer, N., Becker, E., Meier, A., and Sen, B.: Seasonal variations of atmospheric trace gases in the high Arctic at 79°N, Journal of Geophysical Research: Atmospheres, 102, 12 855–12 861, https://doi.org/10.1029/97JD00337, 1997a.

Notholt, J., Toon, G. C., Lehmann, R., Sen, B., and Blavier, J.-F.: Comparison of Arctic and Antarctic trace gas column abundances from ground-based Fourier transform infrared spectrometry, Journal of Geophysical Research: Atmospheres, 102, 12 863–12 869, https://doi.org/10.1029/97JD00358, 1997b.

Notholt, J., Toon, G. C., Rinsland, C. P., Pougatchev, N. S., Jones, N. B., Connor, B. J., Weller, R., Gautrois, M., and Schrems, O.: Latitudinal variations of trace gas concentrations in the free troposphere measured by solar absorption spectroscopy during a ship cruise, Journal of Geophysical Research: Atmospheres, 105, 1337–1349, https://doi.org/10.1029/1999JD900940, 2000.

O'Neill, N. T., Perro, C., Saha, A., Lesins, G., Duck, T. J., Eloranta, E. W., Nott, G. J., Hoffman, A., Karumudi, M. L., Ritter, C., Bourassa, A., Abboud, I., Carn, S. A., and Savastiouk, V.: Properties of Sarychev sulphate aerosols over the Arctic, Journal of Geophysical Research: Atmospheres, 117, https://doi.org/10.1029/2011JD016838, 2012.

Ordóñez, C., Brunner, D., Staehelin, J., Hadjinicolaou, P., Pyle, J. A., Jonas, M., Wernli, H., and Prévôt, A. S. H.: Strong influence of lowermost stratospheric ozone on lower tropospheric background ozone changes over Europe, Geophysical Research Letters, 34, https://doi.org/10.1029/2006GL029113, 2007.

Pan, L. L., Randel, W. J., Gary, B. L., Mahoney, M. J., and Hintsa, E. J.: Definitions and sharpness of the extratropical tropopause: A trace gas perspective, Journal of Geophysical Research: Atmospheres, 109, https://doi.org/10.1029/2004JD004982, 2004.

Parrington, M., Palmer, P. I., Lewis, A. C., Lee, J. D., Rickard, A. R., Carlo, P. D., Taylor, J. W., Hopkins, J. R., Punjabi, S., Oram, D. E., Forster, G., Aruffo, E., Moller, S. J., Bauguitte, S. J.-B., Allan, J. D., Coe, H., and Leigh, R. J.: Ozone photochemistry in boreal biomass burning plumes, Atmospheric Chemistry and Physics, 13, 7321–7341, https://doi.org/10.5194/acp-13-7321-2013, 2013.

Paton-Walsh, C., Jones, N., Wilson, S., Meier, A., Deutscher, N., Griffith, D., Mitchell, R., and Campbell, S.: Trace gas emissions from biomass burning inferred from aerosol optical depth, Geophysical Research Letters, 31, https://doi.org/10.1029/2003GL018973, 2004.

Paton-Walsh, C., Jones, N. B., Wilson, S. R., Haverd, V., Meier, A., Griffith, D. W. T., and Rinsland, C. P.: Measurements of trace gas emissions from Australian forest fires and correlations with coincident measurements of aerosol optical depth, Journal of Geophysical Research: Atmospheres, 110, https://doi.org/10.1029/2005JD006202, 2005.

Paton-Walsh, C., Deutscher, N. M., Griffith, D. W. T., Forgan, B. W., Wilson, S. R., Jones, N. B., and Edwards, D. P.: Trace gas emissions from savanna fires in northern Australia, Journal of Geophysical Research: Atmospheres, 115, https://doi.org/10.1029/2009JD013309, 2010.

https://doi.org/10.5194/acp-2019-881
Preprint. Discussion started: 18 November 2019

Atmospheric Chemistry and Physics Discussions

Patra, P. K., Houweling, S., Krol, M., Bousquet, P., Belikov, D., Bergmann, D., Bian, H., Cameron-Smith, P., Chipperfield, M. P., Corbin, K., Fortems-Cheiney, A., Fraser, A., Gloor, E., Hess, P., Ito, A., Kawa, S. R., Law, R. M., Loh, Z., Maksyutov, S., Meng, L., Palmer, P. I., Prinn, R. G., Rigby, M., Saito, R., and Wilson, C.: TransCom model simulations of CH_4 and related species: Linking transport, surface flux and chemical loss with CH_4 variability in the troposphere and lower stratosphere, Atmospheric Chemistry and Physics, 11, 12 813–12 837, https://doi.org/10.5194/acp-11-12813-2011, 2011.

Peterson, D. A., Campbell, J. R., Hyer, E. J., Fromm, M. D., Kablick, G. P., Cossuth, J. H., and DeLand, M. T.: Wildfire-driven thunderstorms cause a volcano-like stratospheric injection of smoke, Climate and Atmospheric Science, 1, 30, https://doi.org/10.1038/s41612-018-0039-3, 2018.

Petetin, H., Sauvage, B., Parrington, M., Clark, H., Fontaine, A., Athier, G., Blot, R., Boulanger, D., Cousin, J.-M., Nédélec, P., and Thouret, V.: The role of biomass burning as derived from the tropospheric CO vertical profiles measured by IAGOS aircraft in 2002-2017, Atmospheric Chemistry and Physics, 18, 17 277–17 306, https://doi.org/10.5194/acp-18-17277-2018, 2018.

Pougatchev, N. S., Connor, B. J., and Rinsland, C. P.: Infrared measurements of the ozone vertical distribution above Kitt Peak, Journal of Geophysical Research: Atmospheres, 100, 16 689–16 697, https://doi.org/10.1029/95JD01296, 1995.

Ramanathan, V. and Carmichael, G.: Global and regional climate changes due to black carbon, Nature Geoscience, 1, 221–227, https://doi.org/10.1038/ngeo156, 2008.

Rastigejev, Y., Park, R., Brenner, M. P., and Jacob, D. J.: Resolving intercontinental pollution plumes in global models of atmospheric transport, Journal of Geophysical Research: Atmospheres, 115, https://doi.org/10.1029/2009JD012568, 2010.

Rémy, S., Veira, A., Paugam, R., Sofiev, M., Kaiser, J. W., Marenco, F., Burton, S. P., Benedetti, A., Engelen, R. J., Ferrare, R., and Hair, J. W.: Two global data sets of daily fire emission injection heights since 2003, Atmospheric Chemistry and Physics, 17, 2921–2942, https://doi.org/10.5194/acp-17-2921-2017, 2017.

R'Honi, Y., Clarisse, L., Clerbaux, C., Hurtmans, D., Duflot, V., Turquety, S., Ngadi, Y., and Coheur, P.-F.: Exceptional emissions of NH_3 and HCOOH in the 2010 Russian wildfires, Atmospheric Chemistry and Physics, 13, 4171–4181, https://doi.org/10.5194/acp-13-4171-2013, 2013.

Rinsland, C. P., Jones, N. B., Connor, B. J., Logan, J. A., Pougatchev, N. S., Goldman, A., Murcray, F. J., Stephen, T. M., Pine, A. S., Zander, R., Mahieu, E., and Demoulin, P.: Northern and Southern hemisphere ground-based infrared spectroscopic measurements of tropospheric carbon monoxide and ethane, Journal of Geophysical Research: Atmospheres, 103, 28 197–28 217, https://doi.org/10.1029/98JD02515, 1998.

Rodgers, C. D.: Inverse Methods for Atmospheric Sounding: Theory and Practice, Series on Atmospheric, Oceanic and Planetary Physics, World Scientific, 2000.

Rodgers, C. D. and Connor, B. J.: Intercomparison of remote sounding instruments, Journal of Geophysical Research: Atmospheres, 108, 4116, https://doi.org/10.1029/2002JD002299, 2003.

Rodríguez, E., Toledano, C., Cachorro, V. E., Ortiz, P., Stebel, K., Berjón, A., Blindheim, S., Gausa, M., and de Frutos, A. M.: Aerosol characterization at the sub-Arctic site Andenes (69°N, 16°E), by the analysis of columnar optical properties, Quarterly Journal of the Royal Meteorological Society, 138, 471–482, https://doi.org/10.1002/qj.921, 2012.

Rozwadowska, A., Zieliński, T., Petelski, T., and Sobolewski, P.: Cluster analysis of the impact of air back-trajectories on aerosol optical properties at Hornsund, Spitsbergen, Atmospheric Chemistry and Physics, 10, 877–893, https://doi.org/10.5194/acp-10-877-2010, 2010.

Rudolph, J.: The tropospheric distribution and budget of ethane, Journal of Geophysical Research: Atmospheres, 100, 11 369–11 381, https://doi.org/10.1029/95JD00693, 1995.

https://doi.org/10.5194/acp-2019-881
Preprint. Discussion started: 18 November 2019

Atmospheric Chemistry and Physics Discussions

Saha, A., O'Neill, N. T., Eloranta, E., Stone, R. S., Eck, T. F., Zidane, S., Daou, D., Lupu, A., Lesins, G., Shiobara, M., and Others: Pan-Arctic sunphotometry during the ARCTAS-A campaign of April 2008, Geophysical Research Letters, 37, 2010.

Santín, C., Doerr, S. H., Preston, C. M., and González-Rodríguez, G.: Pyrogenic organic matter production from wildfires: A missing sink in the global carbon cycle, Global Change Biology, 21, 1621–1633, https://doi.org/10.1111/gcb.12800, 2015.

Schimel, D. and Baker, D.: Carbon cycle: the wildfire factor, Nature, 420, 29–30, https://doi.org/10.1038/420029a, 2002.

Sharma, S., Lavoué, D., Cachier, H., Barrie, L. A., and Gong, S. L.: Long-term trends of the black carbon concentrations in the Canadian Arctic, Journal of Geophysical Research: Atmospheres, 109, 2004.

Sharma, S., Andrews, E., Barrie, L. A., Ogren, J. A., and Lavoué, D.: Variations and sources of the equivalent black carbon in the high Arctic revealed by long-term observations at Alert and Barrow: 1989–2003, Journal of Geophysical Research: Atmospheres, 111, 2006.

Sharma, S., Ishizawa, M., Chan, D., Lavoué, D., Andrews, E., Eleftheriadis, K., and Maksyutov, S.: 16-year simulation of Arctic black carbon: Transport, source contribution, and sensitivity analysis on deposition, Journal of Geophysical Research: Atmospheres, 118, 943–964, 2013.

Shindell, D. T., Faluvegi, G., Stevenson, D. S., Krol, M. C., Emmons, L. K., Lamarque, J.-F., Pétron, G., Dentener, F. J., Ellingsen, K., Schultz, M. G., Wild, O., Amann, M., Atherton, C. S., Bergmann, D. J., Bey, I., Butler, T., Cofala, J., Collins, W. J., Derwent, R. G., Doherty, R. M., Drevet, J., Eskes, H. J., Fiore, A. M., Gauss, M., Hauglustaine, D. A., Horowitz, L. W., Isaksen, I. S. A., Lawrence, M. G., Montanaro, V., Müller, J.-F., Pitari, G., Prather, M. J., Pyle, J. A., Rast, S., Rodriguez, J. M., Sanderson, M. G., Savage, N. H., Strahan, S. E., Sudo, K., Szopa, S., Unger, N., van Noije, T. P. C., and Zeng, G.: Multimodel simulations of carbon monoxide: Comparison with observations and projected near-future changes, Journal of Geophysical Research: Atmospheres, 111, L01 104, https://doi.org/10.1029/2006JD007100, 2006.

Shindell, D. T., Chin, M., Dentener, F., Doherty, R. M., Faluvegi, G., Fiore, A. M., Hess, P., Koch, D. M., MacKenzie, I. A., Sanderson, M. G., and Others: A multi-model assessment of pollution transport to the Arctic, Atmospheric Chemistry and Physics, 8, 5353–5372, https://doi.org/10.5194/acp-8-5353-2008, 2008.

Singh, H. B.: In situ measurements of HCN and CH_3CN over the Pacific Ocean: Sources, sinks, and budgets, Journal of Geophysical Research: Atmospheres, 108, 8795, https://doi.org/10.1029/2002JD003006, 2003.

Sioris, C. E., Abboud, I., Fioletov, V. E., and McLinden, C. A.: AEROCAN, the Canadian sub-network of AERONET: Aerosol monitoring and air quality applications, Atmospheric Environment, 167, 444–457, https://doi.org/10.1016/j.atmosenv.2017.08.044, 2017.

Sofiev, M., Ermakova, T., and Vankevich, R.: Evaluation of the smoke-injection height from wild-land fires using remote-sensing data, Atmospheric Chemistry and Physics, 12, 1995–2006, https://doi.org/10.5194/acp-12-1995-2012, 2012.

Spivakovsky, C. M., Logan, J. A., Montzka, S. A., Balkanski, Y. J., Foreman-Fowler, M., Jones, D. B. A., Horowitz, L. W., Fusco, A. C., Brenninkmeijer, C. A. M., Prather, M. J., Wofsy, S. C., and McElroy, M. B.: Three-dimensional climatological distribution of tropospheric OH: Update and evaluation, Journal of Geophysical Research: Atmospheres, 105, 8931–8980, https://doi.org/10.1029/1999JD901006, 2000.

Stohl, A.: Characteristics of atmospheric transport into the Arctic troposphere, Journal of Geophysical Research: Atmospheres, 111, https://doi.org/10.1029/2005JD006888, 2006.

Stohl, A., Andrews, E., Burkhart, J. F., Forster, C., Herber, A., Hoch, S. W., Kowal, D., Lunder, C., Mefford, T., Ogren, J. A., Sharma, S., Spichtinger, N., Stebel, K., Stone, R., Ström, J., Tørseth, K., Wehrli, C., and Yttri, K. E.: Pan-Arctic enhancements of light absorbing aerosol concentrations due to North American boreal forest fires during summer 2004, Journal of Geophysical Research: Atmospheres, 111, https://doi.org/10.1029/2006JD007216, 2006.

https://doi.org/10.5194/acp-2019-881
Preprint. Discussion started: 18 November 2019

970 Streets, D. G., Yarber, K. F., Woo, J.-H., and Carmichael, G. R.: Biomass burning in Asia: Annual and seasonal estimates and atmospheric emissions, Global Biogeochemical Cycles, 17, 1099, https://doi.org/10.1029/2003GB002040, 2003.

Sussmann, R. and Buchwitz, M.: Initial validation of ENVISAT/SCIAMACHY columnar CO by FTIR profile retrievals at the Ground-Truthing Station Zugspitze, Atmospheric Chemistry and Physics, 5, 1497–1503, https://doi.org/10.5194/acp-5-1497-2005, 2005.

Sussmann, R. and Schäfer, K.: Infrared spectroscopy of tropospheric trace gases: combined analysis of horizontal and vertical column
975 abundances, Applied Optics, 36, 735–741, https://doi.org/10.1364/AO.36.000735, 1997.

Tanimoto, H., Kajii, Y., Hirokawa, J., Akimoto, H., and Minko, N. P.: The atmospheric impact of boreal forest fires in far eastern Siberia on the seasonal variation of carbon monoxide: Observations at Rishiri, A northern remote island in Japan, Geophysical Research Letters, 27, 4073–4076, https://doi.org/10.1029/2000GL011914, 2000.

Té, Y., Jeseck, P., Franco, B., Mahieu, E., Jones, N., Paton-Walsh, C., Griffith, D. W. T., Buchholz, R. R., Hadji-Lazaro, J., Hurtmans, D., and
980 Janssen, C.: Seasonal variability of surface and column carbon monoxide over the megacity Paris, high-altitude Jungfraujoch and Southern Hemispheric Wollongong stations, Atmospheric Chemistry and Physics, 16, 10 911–10 925, https://doi.org/10.5194/acp-16-10911-2016, 2016.

Teakles, A. D., So, R., Ainslie, B., Nissen, R., Schiller, C., Vingarzan, R., McKendry, I., Macdonald, A. M., Jaffe, D. A., Bertram, A. K., Strawbridge, K. B., Leaitch, W. R., Hanna, S., Toom, D., Baik, J., and Huang, L.: Impacts of the July 2012 Siberian fire plume on air
985 quality in the Pacific Northwest, Atmospheric Chemistry and Physics, 17, 2593–2611, https://doi.org/10.5194/acp-17-2593-2017, 2017.

The International GEOS-Chem User Community: geoschem/geos-chem: GEOS-Chem 12.1.1, https://doi.org/10.5281/zenodo.2249246, 2018.

Thoning, K. W., Tans, P. P., and Komhyr, W. D.: Atmospheric carbon dioxide at Mauna Loa Observatory: 2. Analysis of the NOAA GMCC data, 1974-1985, Journal of Geophysical Research: Atmospheres, 94, 8549–8565, https://doi.org/10.1029/JD094iD06p08549, 1989.

990 Timofeyev, Y., Virolainen, Y., Makarova, M., Poberovsky, A., Polyakov, A., Ionov, D., Osipov, S., and Imhasin, H.: Ground-based spectroscopic measurements of atmospheric gas composition near Saint Petersburg (Russia), Journal of Molecular Spectroscopy, 323, 2–14, https://doi.org/10.1016/j.jms.2015.12.007, 2016.

Tomasi, C., Kokhanovsky, A. A., Lupi, A., Ritter, C., Smirnov, A., O'Neill, N. T., Stone, R. S., Holben, B. N., Nyeki, S., Wehrli, C., Stohl, A., Mazzola, M., Lanconelli, C., Vitale, V., Stebel, K., Aaltonen, V., de Leeuw, G., Rodriguez, E., Herber, A. B., Radionov, V. F., Zielinski,
995 T., Petelski, T., Sakerin, S. M., Kabanov, D. M., Xue, Y., Mei, L., Istomina, L., Wagener, R., McArthur, B., Sobolewski, P. S., Kivi, R., Courcoux, Y., Larouche, P., Broccardo, S., and Piketh, S. J.: Aerosol remote sensing in polar regions, Earth-Science Reviews, 140, 108–157, https://doi.org/10.1016/j.earscirev.2014.11.001, 2015.

Urbanski, S.: Wildland fire emissions, carbon, and climate: Emission factors, Forest Ecology and Management, 317, 51–60, https://doi.org/10.1016/j.foreco.2013.05.045, 2014.

1000 Urbanski, S. P.: Combustion efficiency and emission factors for wildfire-season fires in mixed conifer forests of the northern Rocky Mountains, US, Atmospheric Chemistry and Physics, 13, 7241–7262, https://doi.org/10.5194/acp-13-7241-2013, 2013.

Val Martin, M., Honrath, R. E., Owen, R. C., Pfister, G., Fialho, P., and Barata, F.: Significant enhancements of nitrogen oxides, black carbon, and ozone in the North Atlantic lower free troposphere resulting from North American boreal wildfires, Journal of Geophysical Research: Atmospheres, 111, https://doi.org/10.1029/2006JD007530, 2006.

1005 Val Martin, M., Kahn, R. A., and Tosca, M. G.: A Global Analysis of Wildfire Smoke Injection Heights Derived from Space-Based Multi-Angle Imaging, Remote Sensing, 10, 1609, https://doi.org/10.3390/rs10101609, 2018.

https://doi.org/10.5194/acp-2019-881
Preprint. Discussion started: 18 November 2019

Atmospheric Chemistry and Physics Discussions

van der Werf, G. R., Randerson, J. T., Giglio, L., van Leeuwen, T. T., Chen, Y., Rogers, B. M., Mu, M., van Marle, M. J. E., Morton, D. C., Collatz, G. J., Yokelson, R. J., and Kasibhatla, P. S.: Global fire emissions estimates during 1997–2016, Earth System Science Data, 9, 697–720, https://doi.org/10.5194/essd-9-697-2017, 2017.

Veraverbeke, S., Rogers, B. M., Goulden, M. L., Jandt, R. R., Miller, C. E., Wiggins, E. B., and Randerson, J. T.: Lightning as a major driver of recent large fire years in North American boreal forests, Nature Climate Change, 7, 529–534, https://doi.org/10.1038/nclimate3329, 2017.

Viatte, C., Strong, K., Paton-Walsh, C., Mendonca, J., O'Neill, N. T., and Drummond, J. R.: Measurements of CO, HCN, and C_2H_6 total columns in smoke plumes transported from the 2010 Russian boreal forest fires to the Canadian high Arctic, Atmosphere-Ocean, 51, 522–531, https://doi.org/10.1080/07055900.2013.823373, 2013.

Viatte, C., Strong, K., Walker, K. A., and Drummond, J. R.: Five years of CO, HCN, C_2H_6, C_2H_2, CH_3OH, HCOOH and H_2CO total columns measured in the Canadian high Arctic, Atmospheric Measurement Techniques, 7, 1547–1570, https://doi.org/10.5194/amt-7-1547-2014, 2014.

Viatte, C., Strong, K., Hannigan, J., Nussbaumer, E., Emmons, L. K., Conway, S., Paton-Walsh, C., Hartley, J., Benmergui, J., and Lin, J.: Identifying fire plumes in the Arctic with tropospheric FTIR measurements and transport models, Atmospheric Chemistry and Physics, 15, 2227–2246, https://doi.org/10.5194/acp-15-2227-2015, 2015.

Vigouroux, C., Stavrakou, T., Whaley, C., Dils, B., Duflot, V., Hermans, C., Kumps, N., Metzger, J.-M., Scolas, F., Vanhaelewyn, G., Müller, J.-F., Jones, D. B. A., Li, Q., and De Mazière, M.: FTIR time-series of biomass burning products (HCN, C_2H_6, C_2H_2, CH_3OH, and HCOOH) at Reunion Island (21°S, 55°E) and comparisons with model data, Atmospheric Chemistry and Physics, 12, 10 367–10 385, https://doi.org/10.5194/acp-12-10367-2012, 2012.

Wang, Q., Jacob, D. J., Fisher, J. A., Mao, J., Leibensperger, E. M., Carouge, C. C., Sager, P. L., Kondo, Y., Jimenez, J. L., Cubison, M. J., and Others: Sources of carbonaceous aerosols and deposited black carbon in the Arctic in winter-spring: Implications for radiative forcing, Atmospheric Chemistry and Physics, 11, 12 453–12 473, https://doi.org/10.5194/acp-11-12453-2011, 2011.

Ward, D. E. and Hardy, C. C.: Smoke emissions from wildland fires, Environment International, 17, 117–134, https://doi.org/10.1016/0160-4120(91)90095-8, 1991.

Warneke, C., Bahreini, R., Brioude, J., Brock, C. A., de Gouw, J. A., Fahey, D. W., Froyd, K. D., Holloway, J. S., Middlebrook, A., Miller, L., Montzka, S., Murphy, D. M., Peischl, J., Ryerson, T. B., Schwarz, J. P., Spackman, J. R., and Veres, P.: Biomass burning in Siberia and Kazakhstan as an important source for haze over the Alaskan Arctic in April 2008, Geophysical Research Letters, 36, https://doi.org/10.1029/2008GL036194, 2009.

Wentworth, G. R., Aklilu, Y.-A., Landis, M. S., and Hsu, Y.-M.: Impacts of a large boreal wildfire on ground level atmospheric concentrations of PAHs, VOCs and ozone, Atmospheric Environment, 178, 19–30, https://doi.org/10.1016/j.atmosenv.2018.01.013, 2018.

Westerling, A. L., Hidalgo, H. G., Cayan, D. R., and Swetnam, T. W.: Warming and earlier spring increase western US forest wildfire activity, Science, 313, 940–943, https://doi.org/10.1126/science.1128834, 2006.

Whaley, C. H., Strong, K., Jones, D. B. A., Walker, T. W., Jiang, Z., Henze, D. K., Cooke, M. A., McLinden, C. A., Mittermeier, R. L., Pommier, M., and Fogal, P. F.: Toronto area ozone: Long-term measurements and modeled sources of poor air quality events, Journal of Geophysical Research: Atmospheres, 120, 11,368–11,390, https://doi.org/10.1002/2014JD022984, 2015.

Wiacek, A., Taylor, J. R., Strong, K., Saari, R., Kerzenmacher, T. E., Jones, N. B., and Griffith, D. W. T.: Ground-Based Solar Absorption FTIR Spectroscopy: Characterization of Retrievals and First Results from a Novel Optical Design Instrument at a New NDACC Complementary Station, Journal of Atmospheric and Oceanic Technology, 24, 432–448, https://doi.org/10.1175/JTECH1962.1, 2007.

Winiger, P., Barrett, T. E., Sheesley, R. J., Huang, L., Sharma, S., Barrie, L. A., Yttri, K. E., Evangeliou, N., Eckhardt, S., Stohl, A., Klimont, Z., Heyes, C., Semiletov, I. P., Dudarev, O. V., Charkin, A., Shakhova, N., Holmstrand, H., Andersson, A., and Gustafsson, Ö.: Source apportionment of circum-Arctic atmospheric black carbon from isotopes and modeling, Science Advances, 5, 8052, https://doi.org/10.1126/sciadv.aau8052, 2019.

Witte, J. C., Douglass, A. R., Silva, A. d., Torres, O., Levy, R., and Duncan, B. N.: NASA A-Train and Terra observations of the 2010 Russian wildfires, Atmospheric Chemistry and Physics, 11, 9287–9301, 2011.

Wotton, B. M., Nock, C. A., and Flannigan, M. D.: Forest fire occurrence and climate change in Canada, International Journal of Wildland Fire, 19, 253–271, https://doi.org/10.1071/WF09002, 2010.

Xiao, Y., Logan, J. A., Jacob, D. J., Hudman, R. C., Yantosca, R., and Blake, D. R.: Global budget of ethane and regional constraints on U.S. sources, Journal of Geophysical Research: Atmospheres, 113, https://doi.org/10.1029/2007JD009415, 2008.

Yasunari, T. J., Kim, K.-M., da Silva, A. M., Hayasaki, M., Akiyama, M., and Murao, N.: Extreme air pollution events in Hokkaido, Japan, traced back to early snowmelt and large-scale wildfires over East Eurasia: Case studies, Scientific Reports, 8, 6413, https://doi.org/10.1038/s41598-018-24335-w, 2018.

Yevich, R. and Logan, J. A.: An assessment of biofuel use and burning of agricultural waste in the developing world, Global Biogeochemical Cycles, 17, 1095, https://doi.org/10.1029/2002GB001952, 2003.

Yokelson, R. J., Griffith, D. W. T., and Ward, D. E.: Open-path Fourier transform infrared studies of large-scale laboratory biomass fires, Journal of Geophysical Research: Atmospheres, 101, 21 067–21 080, 1996.

Yokelson, R. J., Goode, J. G., Ward, D. E., Susott, R. A., Babbitt, R. E., Wade, D. D., Bertschi, I., Griffith, D. W. T., and Hao, W. M.: Emissions of formaldehyde, acetic acid, methanol, and other trace gases from biomass fires in North Carolina measured by airborne Fourier transform infrared spectroscopy, Journal of Geophysical Research: Atmospheres, 104, 30 109–30 125, https://doi.org/10.1029/1999JD900817, 1999.

Yokelson, R. J., Bertschi, I. T., Christian, T. J., Hobbs, P. V., Ward, D. E., and Hao, W. M.: Trace gas measurements in nascent, aged, and cloud-processed smoke from African savanna fires by airborne Fourier transform infrared spectroscopy (AFTIR), Journal of Geophysical Research: Atmospheres, 108, 8478, https://doi.org/10.1029/2002JD002322, 2003.

Yokelson, R. J., Crounse, J. D., DeCarlo, P. F., Karl, T., Urbanski, S., Atlas, E, Campos, T., Shinozuka, Y., Kapustin, V., Clarke, A. D., Weinheimer, A., Knapp, D. J., Montzka, D. D., Holloway, J., Weibring, P., Flocke, F., Zheng, W., Toohey, D., Wennberg, P. O., Wiedinmyer, C., Mauldin, L., Fried, A., Richter, D., Walega, J., Jimenez, J. L., Adachi, K., Buseck, P. R., Hall, S. R., and Shetter, R.: Emissions from biomass burning in the Yucatan, Atmospheric Chemistry and Physics, 9, 5785–5812, https://doi.org/10.5194/acp-9-5785-2009, 2009.

Yokelson, R. J., Andreae, M. O., and Akagi, S. K.: Pitfalls with the use of enhancement ratios or normalized excess mixing ratios measured in plumes to characterize pollution sources and aging, Atmospheric Measurement Techniques, 6, 2155–2158, https://doi.org/10.5194/amt-6-2155-2013, 2013.

York, D., Evensen, N. M., Martińez, M. L., and De Basabe Delgado, J.: Unified equations for the slope, intercept, and standard errors of the best straight line, American Journal of Physics, 72, 367–375, https://doi.org/10.1119/1.1632486, 2004.

Yurganov, L. N.: A quantitative assessment of the 1998 carbon monoxide emission anomaly in the Northern Hemisphere based on total column and surface concentration measurements, Journal of Geophysical Research: Atmospheres, 109, https://doi.org/10.1029/2004JD004559, 2004.

Yurganov, L. N., Duchatelet, P., Dzhola, A. V., Edwards, D. P., Hase, F., Kramer, I., Mahieu, E., Mellqvist, J., Notholt, J., Novelli, P. C., Rockmann, A., Scheel, H. E., Schneider, M., Schulz, A., Strandberg, A., Sussmann, R., Tanimoto, H., Velazco, V., Drummond, J. R., and

https://doi.org/10.5194/acp-2019-881
Preprint. Discussion started: 18 November 2019

Gille, J. C.: Increased Northern Hemispheric carbon monoxide burden in the troposphere in 2002 and 2003 detected from the ground and from space, Atmospheric Chemistry and Physics, 5, 563–573, https://doi.org/10.5194/acp-5-563-2005, 2005.

Yurganov, L. N., Rakitin, V., Dzhola, A., August, T., Fokeeva, E., George, M., Gorchakov, G., Grechko, E., Hannon, S., Karpov, A., Ott, L., Semutnikova, E., Shumsky, R., and Strow, L.: Satellite and ground-based CO total column observations over 2010 Russian fires: accuracy of top-down estimates based on thermal IR satellite data, Atmospheric Chemistry and Physics, 11, 7925–7942, https://doi.org/10.5194/acp-11-7925-2011, 2011.

Zander, R., Mahieu, E., Demoulin, P., Duchatelet, P., Roland, G., Servais, C., De Mazière, M., Reimann, S., and Rinsland, C. P.: Our changing atmosphere: evidence based on long-term infrared solar observations at the Jungfraujoch since 1950, The Science of the Total Environment, 391, 184–195, https://doi.org/10.1016/j.scitotenv.2007.10.018, 2008.

Zellweger, C., Hüglin, C., Klausen, J., Steinbacher, M., Vollmer, M., and Buchmann, B.: Inter-comparison of four different carbon monoxide measurement techniques and evaluation of the long-term carbon monoxide time series of Jungfraujoch, Atmospheric Chemistry and Physics, 9, 3491–3503, https://doi.org/10.5194/acp-9-3491-2009, 2009.

Zhao, Y., Kondo, Y., Murcray, F. J., Liu, X., Koike, M., Kita, K., Nakajima, H., Murata, I., and Suzuki, K.: Carbon monoxide column abundances and tropospheric concentrations retrieved from high resolution ground-based infrared solar spectra at 43.5°N over Japan, Journal of Geophysical Research: Atmospheres, 102, 23 403–23 411, https://doi.org/10.1029/97JD01970, 1997.

Zhao, Y., Kondo, Y., Murcray, F. J., Liu, X., Koike, M., Irie, H., Strong, K., Suzuki, K., Sera, M., and Ikegami, Y.: Seasonal variations of HCN over Northern Japan measured by ground-based infrared solar spectroscopy, Geophysical Research Letters, 27, 2085–2088, https://doi.org/10.1029/1999GL011218, 2000.

Zhao, Y., Strong, K., Kondo, Y., Koike, M., Matsumi, Y., Irie, H., Rinsland, C. P., Jones, N. B., Suzuki, K., Nakajima, H., Nakane, H., and Murata, I.: Spectroscopic measurements of tropospheric CO, C_2H_6, C_2H_2, and HCN in Northern Japan, Journal of Geophysical Research: Atmospheres, 107, 4343–4359, https://doi.org/10.1029/2001JD000748, 2002.

https://doi.org/10.5194/acp-2019-881
Preprint. Discussion started: 18 November 2019

Atmospheric Chemistry and Physics Discussions
Open Access
EGU

Table 1. Summary of NDACC and AERONET sites used in this study.

	Site	Latitude, Longitude	Elevation [m a.s.l.]	Measurement Years	Key References
NDACC	**Eureka**	80.05°N, 86.42°W	610	2006-2018	Batchelor et al., 2009; Lutsch et al., 2016, 2019, Viatte et al., 2013, 2014, 2015
AERONET	PEARL	80.05°N, 86.42°W	610	2007-2018	Saha et al., 2010; O'Neill et al., 2012
	Ny-Ålesund	78.92°N, 11.93°E	15	1992-2018	Notholt et al., 1997a, b, 2000
	Horsund	77.00°N, 86.42°W	12	2004-2018	Rozwadowska et al., 2010
	Thule	76.53°N, 68.74°W	225	1999-2018	Hannigan et al., 2009; Viatte et al., 2015 Lutsch et al., 2019
	Thule	76.52°N, 68.77°W	225	2007-2018	Tomasi et al., 2015
	Kiruna	67.84°N, 20.41°E	419	1996-2018	Blumenstock et al., 1997, 2009
	Andenes	69.28°N, 16.01°E	379	2002-2018	Rodríguez et al., 2012
	Poker Flat	65°N, 142°W	610	1999-2011	Kasai et al., 2005a, b
	Bonanza Creek	65.74°N, 148/32°W	353	1994-2018	Eck et al., 2009
	St. Petersburg	59.88°N, 29.83°E	20	2009-2018	Makarova et al., 2011; Timofeyev et al., 2016
	Toravere	58.27°N, 26.47°E	85	2002-2018	Arola et al., 2007
	Zugspitze	47.42°N, 10.98°E	2964	1995-2018	Sussmann and Schäfer, 1997, Sussmann and Buchwitz, 2005
	Davos	46.81°N, 9.84°E	1589	2001-2018	Gubler et al., 2012
	Jungfraujoch	46.55°N, 7.98°E	3580	1984-2018	Mahieu et al., 1997; Zander et al., 2008,
	Davos	46.81°N, 9.84°E	1589	2001-2018	Gubler et al., 2012
	Toronto	43.66°N, 79.40°W	174	2002-2018	Wiacek et al., 2007; Whaley et al., 2015, Lutsch et al., 2016
	Toronto	43.79°N, 79.47°E	186	1996-2018	Sioris et al., 2017
	Rikubetsu	43.46°N, 143.77°E	380	2002-2018	Zhao et al., 1997, 2000, 2002
	Noto	37.34°N, 137.14°E	200	2001-2018	Makar et al., 2018

https://doi.org/10.5194/acp-2019-881
Preprint. Discussion started: 18 November 2019

Atmospheric Chemistry and Physics Discussions

Table 2. Summary of the source regions used in the GEOS-Chem tagged CO simulation.

Type	Name	Description
Anthropogenic	NA	North America
	EU	Europe
	AS	Asia
	ROW	Rest of World
Biomass Burning	BONA	Boreal North America
	TENA	Temperate North America
	CEAM	Central America
	NHSA	Northern Hemisphere South America
	SHSA	Southern Hemisphere South America
	EURO	Europe
	MIDE	Middle East
	NHAF	Northern Hemisphere Africa
	SHAF	Southern Hemisphere Africa
	BOAS	Boreal Asia
	CEAS	Central East Asia
	SEAS	Southeast Asia
	EQAS	Equatorial Asia
	AUST	Australia and New Zealand
Other	CH_4	Methane oxidation
	NMVOC	Non-methane volatile organic compound oxidation

https://doi.org/10.5194/acp-2019-881
Preprint. Discussion started: 18 November 2019

Atmospheric Chemistry and Physics Discussions

Table 3. Summary of wildfire pollution event detection criteria for all sites.

Site	CO Enhancement[a] Detection Threshold [σ]	Event Separation[b] [days]	$EnhR_{HCN}$[c] Minimum r	$EnhR_{C_2H_6}$[d] Minimum r
Eureka	1.0	7	0.5	0.5
Ny-Ålesund[e]	1.0	14	–	–
Thule	1.0	7	0.5	0.5
Kiruna	1.0	7	0.5	0.5
Poker Flat[e]	1.0	7	–	–
St. Petersburg	1.0	10	0.5	0.5
Zugspitze	1.0	7	0.5	0.5
Jungfraujoch	1.0	7	0.5	0.5
Toronto	1.0	8	0.5	0.5
Rikubetsu[e]	2.0	14	–	–

[a] Threshold for detection of enhanced CO measurements.

[b] Time separation between detected CO enhancements to categorize individual events.

[c] Minimum correlation coefficient r for $EnhR_{HCN}$.

[d] Minimum correlation coefficient r for $EnhR_{C_2H_6}$.

[e] No criteria applied for enhancements ratios due to a lack of coincident CO, HCN and C_2H_6.

https://doi.org/10.5194/acp-2019-881
Preprint. Discussion started: 18 November 2019

Atmospheric Chemistry and Physics Discussions

Table 4. Number of measurements of CO, HCN and C_2H_6 for all sites from 2003-2018 unless otherwise stated. Number of pairs of HCN and C_2H_6 with CO in the 1-hr window is also shown with the mean time difference between paired measurements (Δt).

Site	CO	HCN	HCN:CO	Δt [min]	C_2H_6	C_2H_6:CO	Δt [min]
Eureka[a]	5411	4674	4352	10	3578	3316	11
NyAlesund	1349	1115	512	28	1129	541	25
Thule	6369	2586	1399	22	3894	1782	11
Kiruna	1999	1866	1597	15	2650	1883	32
Poker Flat[b]	2602	1791	1432	24	1638	1343	28
St. Petersburg [c]	4289	3846	2552	31	4154	3706	0[d]
Jungfraujoch	4844	3244	2409	31	11372	6572	34
Zugspitze[e]	19445	903	895	17	13539	13307	8
Toronto	3779	2978	2104	33	4276	2877	22
Rikubetsu	1199	1105	784	19	1057	633	31

[a] From 2006-2018.

[b] From 2003-2011.

[c] From 2009-2018.

[d] St. Petersburg uses two non-standard broadband filters and therefore CO and C_2H_6 measurements occur simultaneously.

[e] Zugspitze HCN measurements began in 2015 while CO and C_2H_6 measurements are reported from 2003-2018.

https://doi.org/10.5194/acp-2019-881
Preprint. Discussion started: 18 November 2019

Atmospheric Chemistry and Physics Discussions

1105 **Table 5.** Mean enhancement ratios of HCN and C_2H_6 for BONA and BOAS for all detected wildfire events. The value in parenthesis is the 1σ standard deviation of the mean. The number of detected events for each site and source are also given.

	BONA			BOAS		
Site	Nr.	HCN	C_2H_6	Nr.	HCN	C_2H_6
Eureka	9	0.007 (0.003)	0.012 (0.005)	10	0.008 (0.004)	0.013 (0.003)
Ny-Ålesund	9	–	–	6	–	–
Thule	13	0.007 (0.004)	0.010 (0.003)	4	0.009 (0.002)	0.012 (0.003)
Kiruna	4	0.005 (0.002)	0.014 (0.010)	8	0.005 (0.001)	0.016 (0.010)
Poker Flat	8	–	–	5	–	–
St. Petersburg	1	0.004	0.005	3	0.004 (0.001)	0.019 (0.014)
Zugspitze	1	0.003	0.012	1	0.001	0.001
Jungfraujoch	8	0.006 (0.005)	0.015 (0.014)	9	0.004 (0.002)	0.012 (0.004)
Toronto	4	0.010 (0.008)	0.023 (0.008)	1	0.007	0.028
Rikubetsu	0	–	–	11	–	–

https://doi.org/10.5194/acp-2019-881
Preprint. Discussion started: 18 November 2019

Atmospheric Chemistry and Physics Discussions

Table 6. Monthly-mean relative difference of GEOS-Chem minus FTIR [(model-FTIR)/FTIR] CO tropospheric partial columns over all years for measurements from 2003-2018.

Site	Jan.	Feb.	Mar.	Apr.	May	Jun.	Jul.	Aug.	Sep.	Oct.	Nov.	Dec.	**Yearly**
Eureka	–	-3.5	-2.6	-1.3	5.0	1.7	2.2	-6.5	-8.0	-7.5	–	–	-1.5
Ny-Ålesund	–	–	-4.2	-2.4	0.1	4.3	2.1	-2.5	-3.8	–	–	–	-0.8
Thule	–	3.2	-4.0	-4.6	0.5	-0.2	1.5	-6.1	-10.0	-6.8	–	–	-3.0
Kiruna	-5.6	-4.5	-6.2	-7.3	-7.6	-6.0	-9.7	-14.6	-12.3	-6.4	1.7	–	-7.6
Poker Flat	–	-23.9	-22.2	-22.0	-16.2	-15.5	-15.2	-21.3	-24.3	-19.3	-9.2	–	-19.4
Peterhof	-0.6	-0.9	-1.8	-4.9	-4.7	-4.3	-7.7	-12.2	-10.1	-2.0	2.5	4.7	-5.2
Zugspitze	-14.4	-15.7	-18.2	-20.2	-19.9	-19.0	-21.3	-21.8	-17.3	-13.2	-12.3	-11.9	-16.9
Jungfraujoch	-21.6	-21.5	-24.0	-25.0	-24.8	-22.3	-24.9	-23.6	-21.4	-18.6	-18.5	-18.7	-22.3
Toronto	-1.0	-2.2	-6.6	-7.8	-8.4	-8.5	-11.3	-11.4	-9.3	-5.0	-0.4	-0.0	-7.2
Rikubetsu	-5.4	-6.9	-2.8	-1.8	-0.9	-14.3	-14.0	-17.4	-15.0	-8.1	1.9	-1.9	-7.2

https://doi.org/10.5194/acp-2019-881
Preprint. Discussion started: 18 November 2019

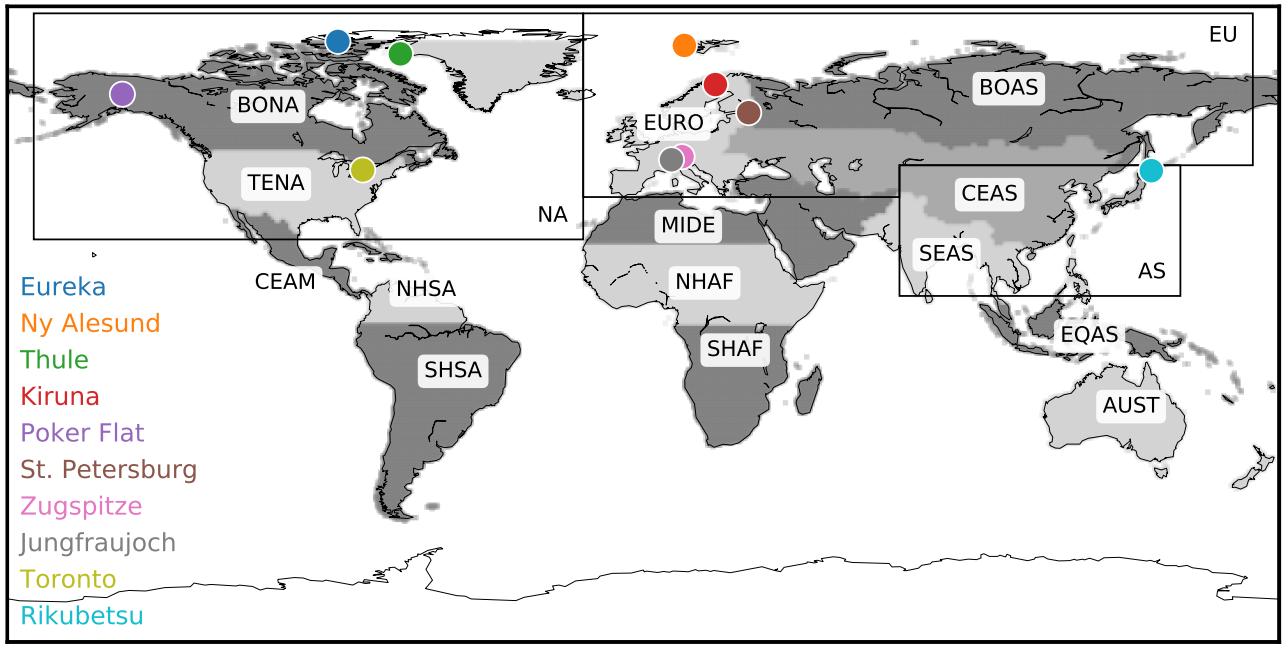

Figure 1. Locations of ground-based FTIR sites used in this study. The biomass burning regions (shaded), and anthropogenic source regions (black rectangles) used for the GEOS-Chem tagged CO simulation are also shown and summarized in Table 2.

https://doi.org/10.5194/acp-2019-881
Preprint. Discussion started: 18 November 2019

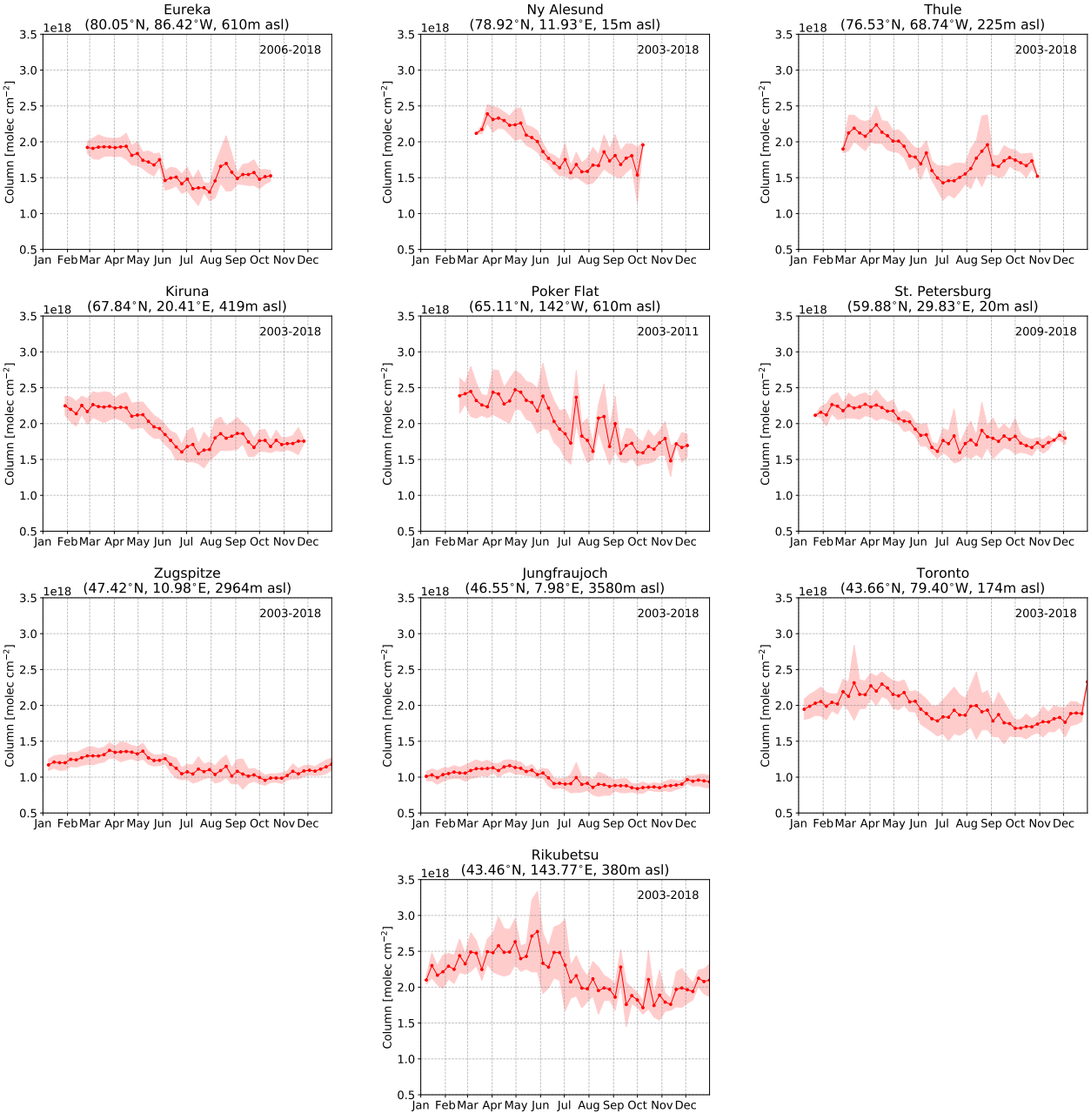

Figure 2. Weekly-mean CO tropospheric partial columns taken over all years of measurements at each site. The years included in the mean are listed in the top right corner of each panel. The shaded region represents a 1σ standard deviation from the mean.

https://doi.org/10.5194/acp-2019-881
Preprint. Discussion started: 18 November 2019

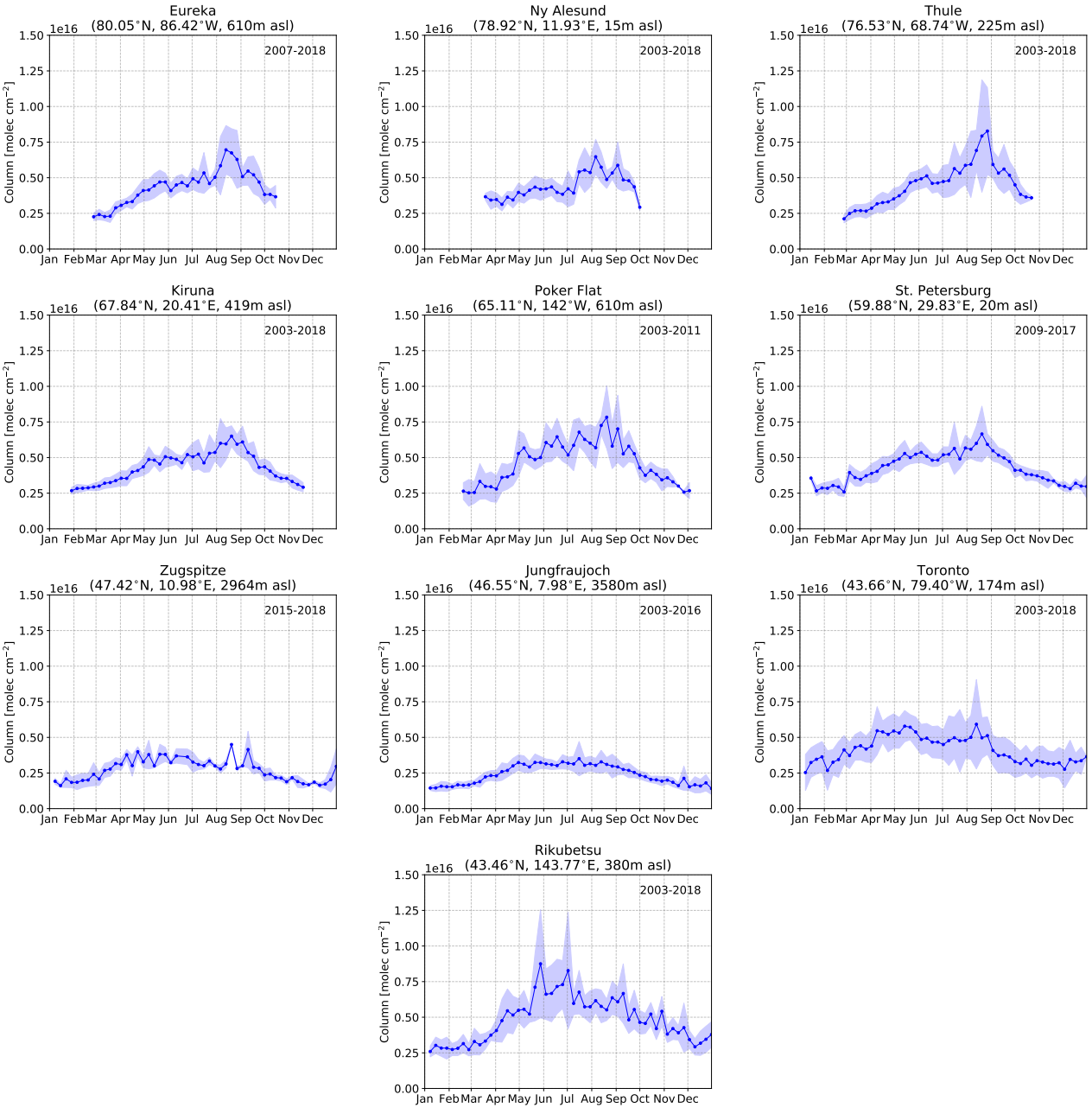

Figure 3. Same as Fig. 2 but for HCN.

https://doi.org/10.5194/acp-2019-881
Preprint. Discussion started: 18 November 2019

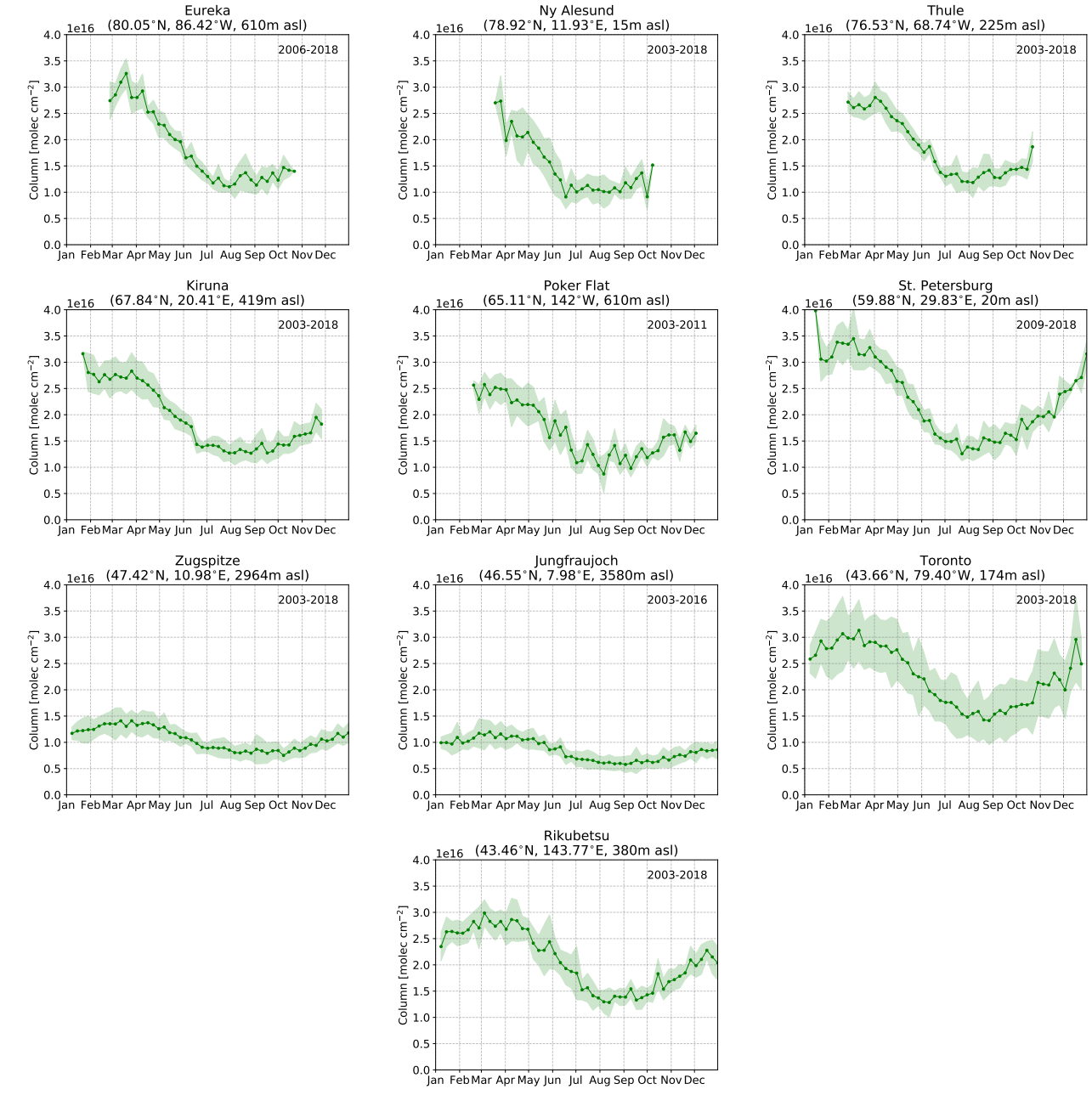

Figure 4. Same as Fig. 2 but for C_2H_6.

https://doi.org/10.5194/acp-2019-881
Preprint. Discussion started: 18 November 2019

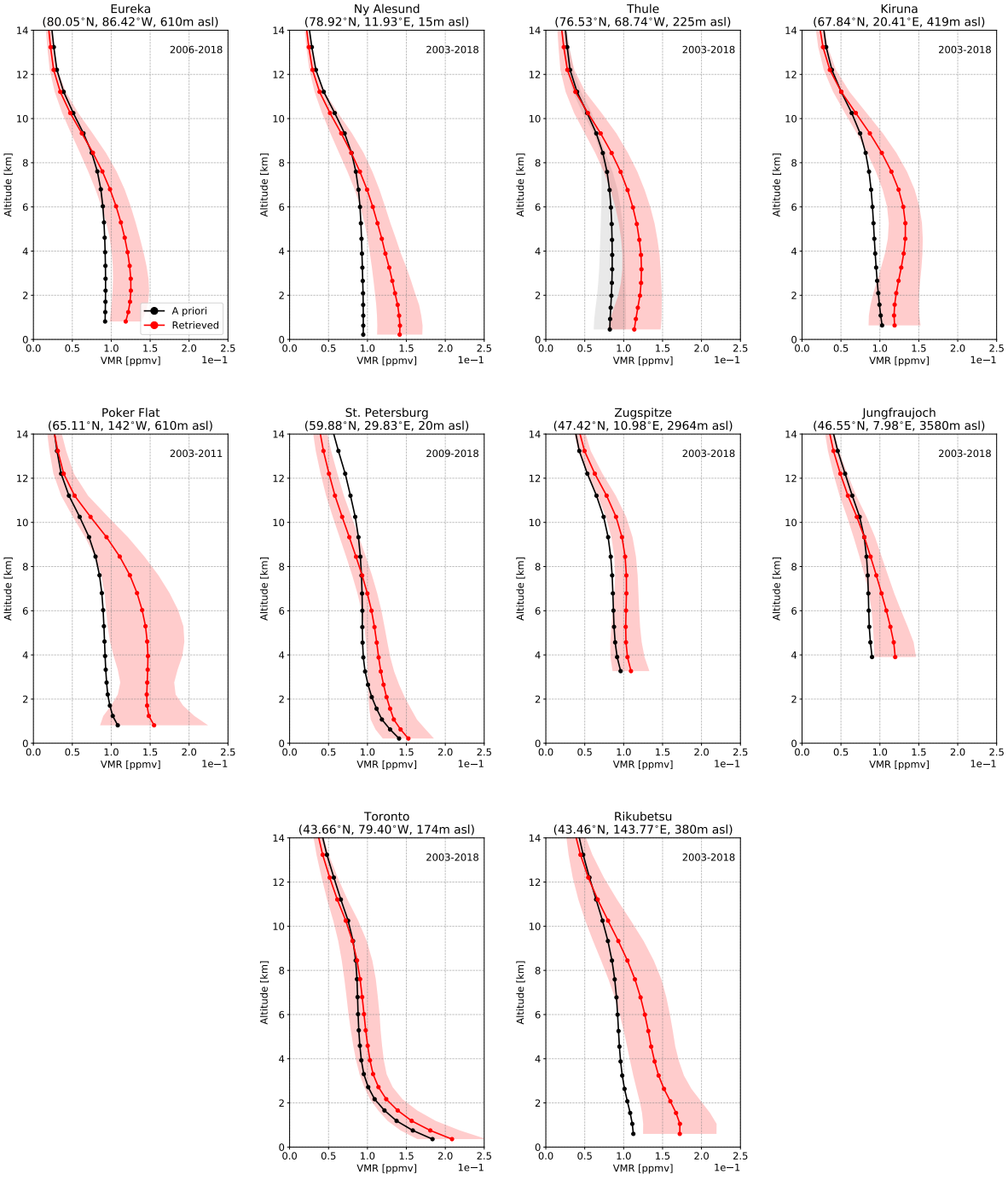

Figure 5. Mean retrieved (red) and a priori (black) VMR profiles of CO taken over all years of measurements at each site. The shaded region indicates the 1σ standard deviation from the mean. The circle markers indicate the layer centers of the FTIR vertical retrieval grid.

https://doi.org/10.5194/acp-2019-881
Preprint. Discussion started: 18 November 2019

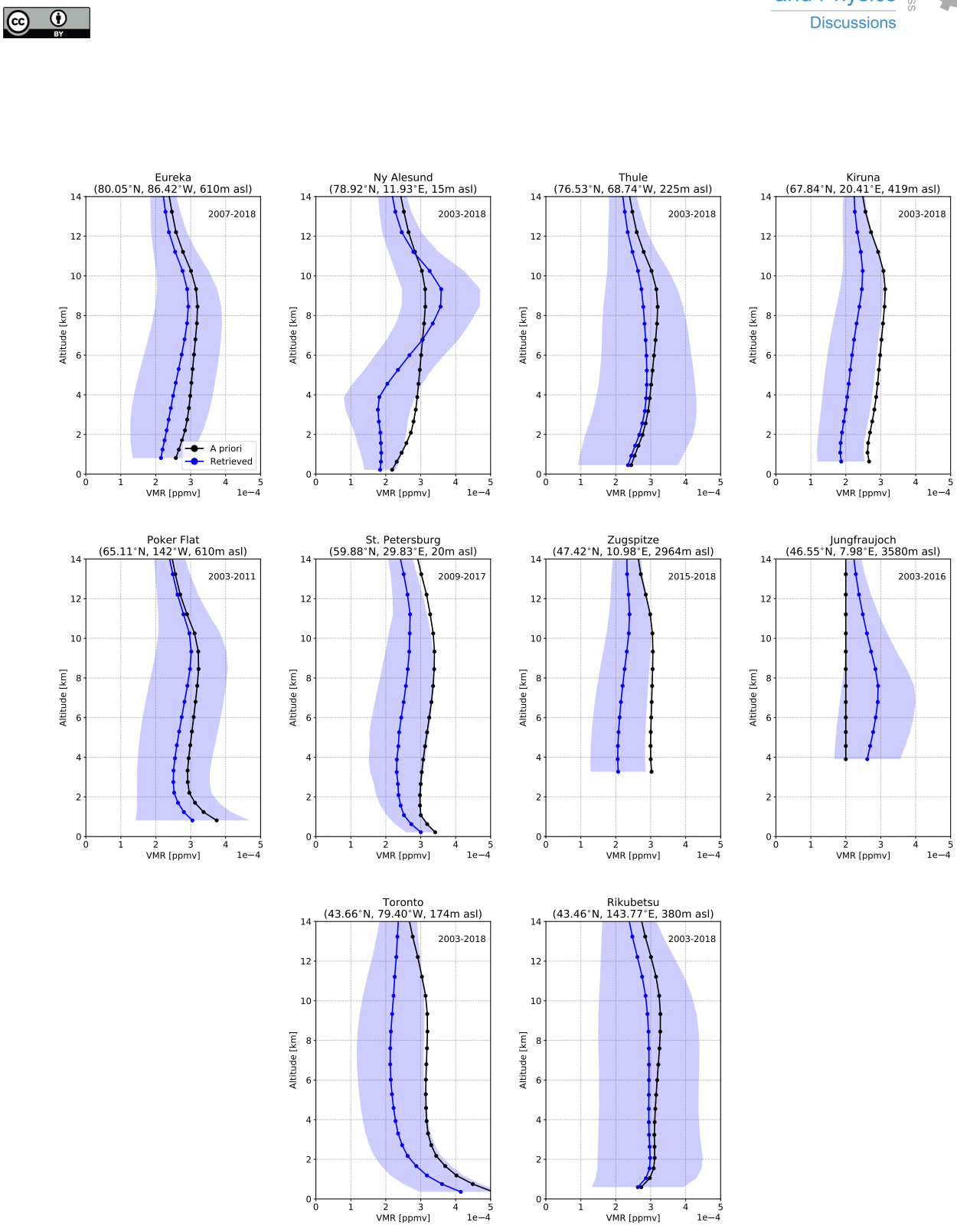

Figure 6. Same as Fig. 5 but for HCN.

https://doi.org/10.5194/acp-2019-881
Preprint. Discussion started: 18 November 2019

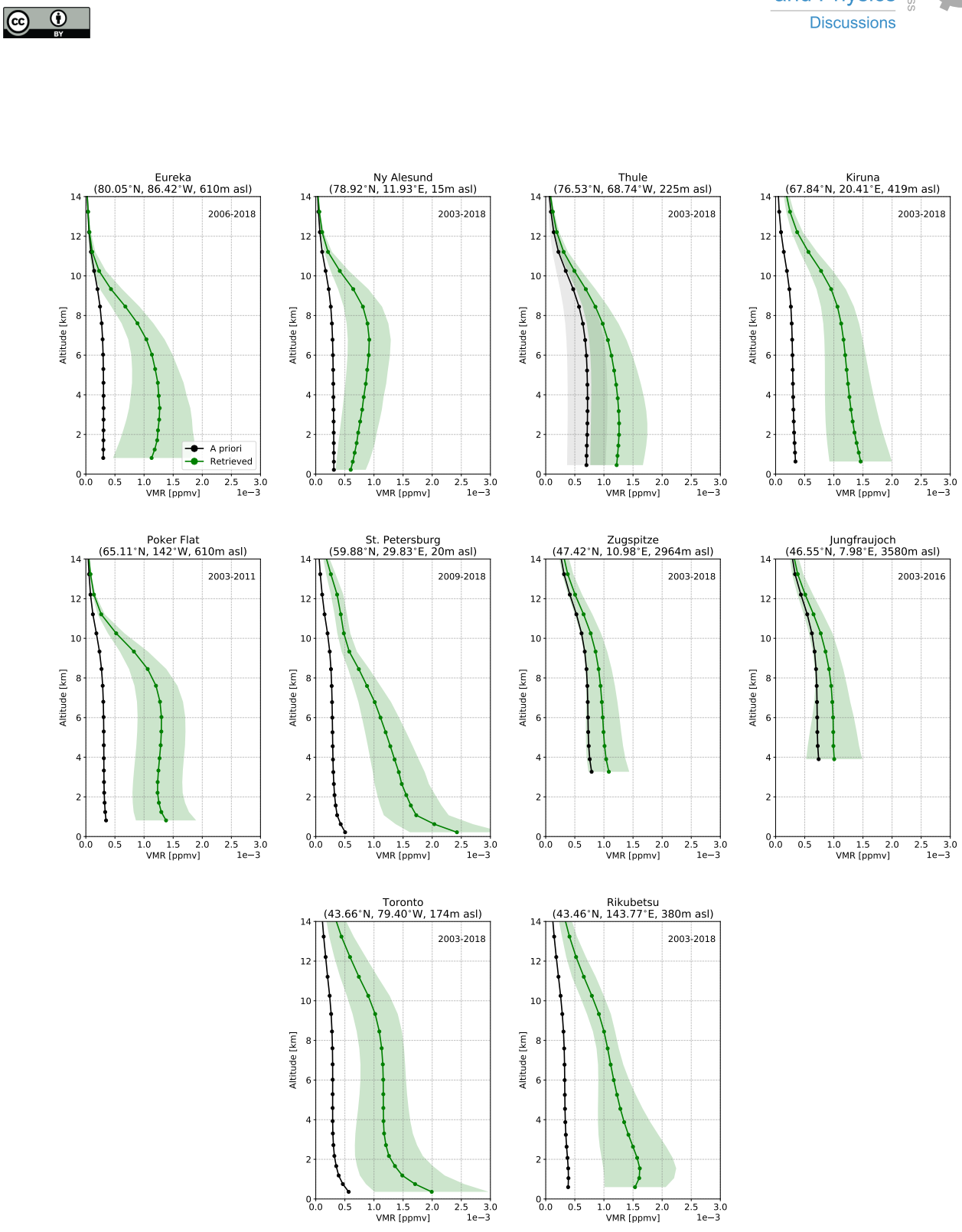

Figure 7. Same as Fig. 5 but for C_2H_6

https://doi.org/10.5194/acp-2019-881
Preprint. Discussion started: 18 November 2019

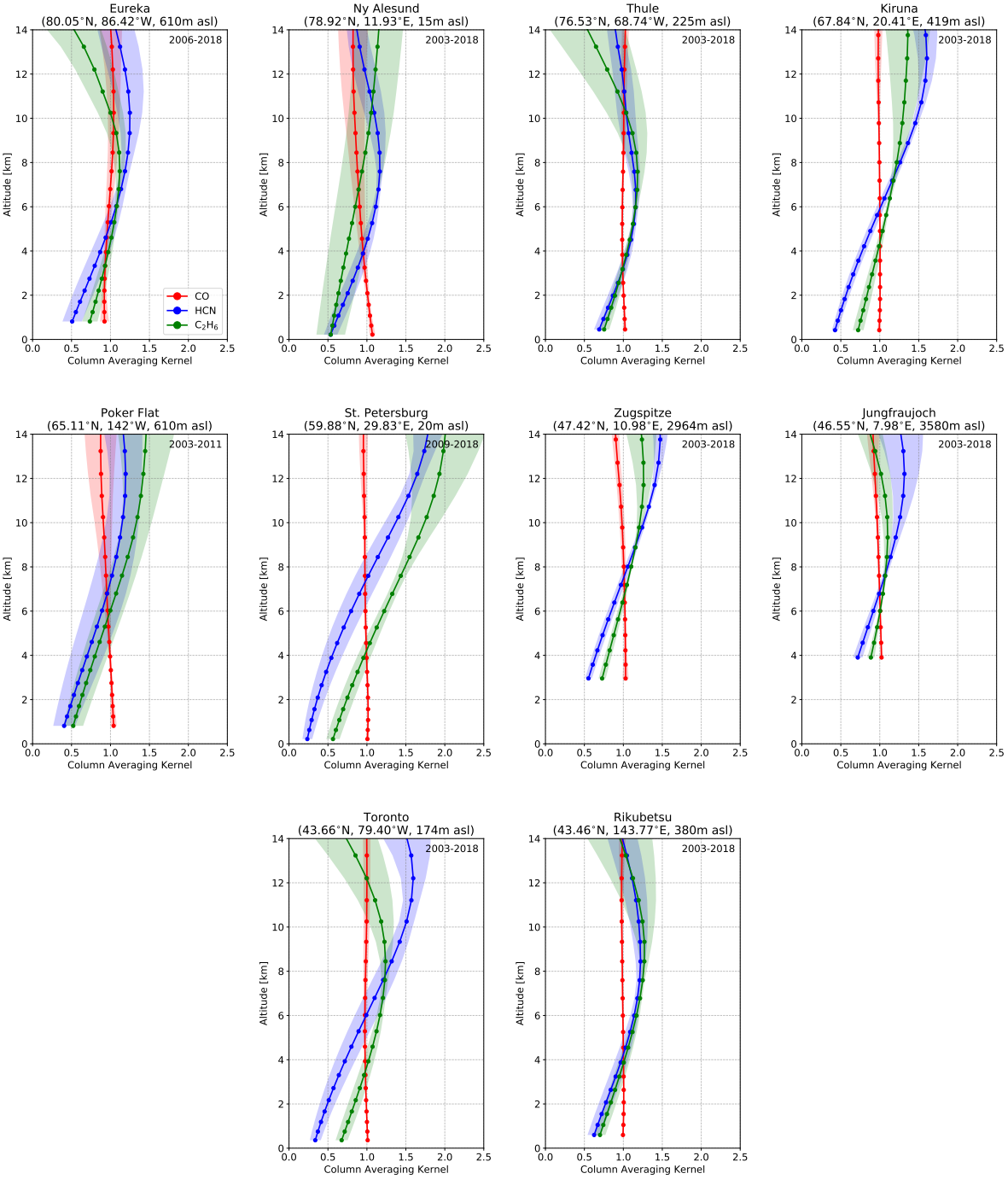

Figure 8. Mean CO, HCN and C_2H_6 normalized total column averaging kernels in units of molec cm^{-2}/ molec cm^{-2}, taken over all years of measurements at each site. The shaded region indicates a 1σ standard deviation from the mean. The circle markers indicate the layer centers of the FTIR vertical retrieval grid.

https://doi.org/10.5194/acp-2019-881
Preprint. Discussion started: 18 November 2019

Atmospheric Chemistry and Physics Discussions

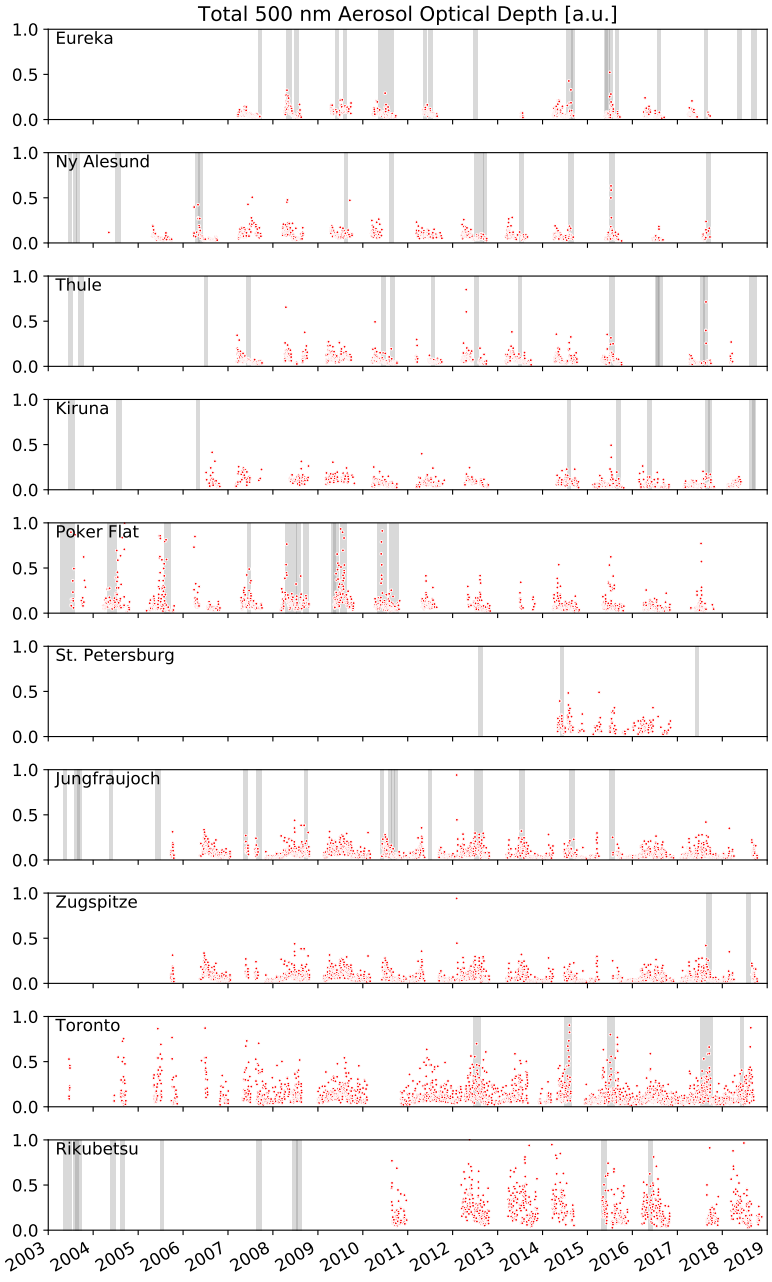

Figure 9. Total 500 nm aerosol optical depth from the adjacent AERONET sites listed in Table 1. The grey shaded regions indicated the period of fire-affected measurements detected at each FTIR site.

https://doi.org/10.5194/acp-2019-881
Preprint. Discussion started: 18 November 2019

Atmospheric Chemistry and Physics Discussions

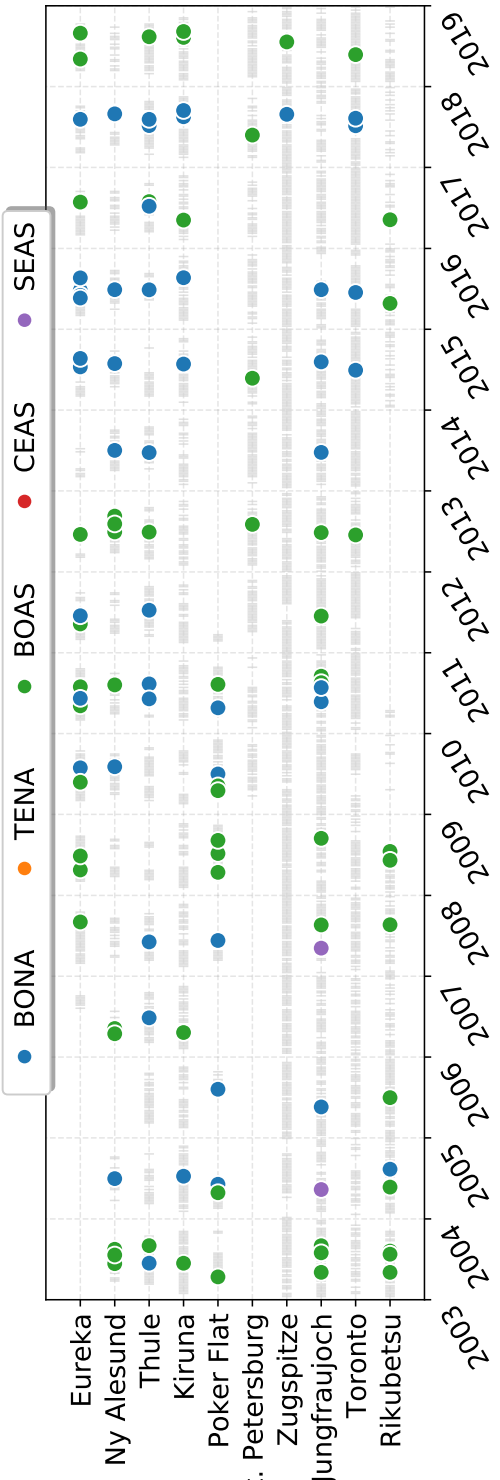

Figure 10. Summary of detected wildfire pollution events. The grey bars indicate periods of CO measurements and the coloured points represent the identified wildfire pollution events and their respective source attributed by the GEOS-Chem tagged CO simulation.

https://doi.org/10.5194/acp-2019-881
Preprint. Discussion started: 18 November 2019

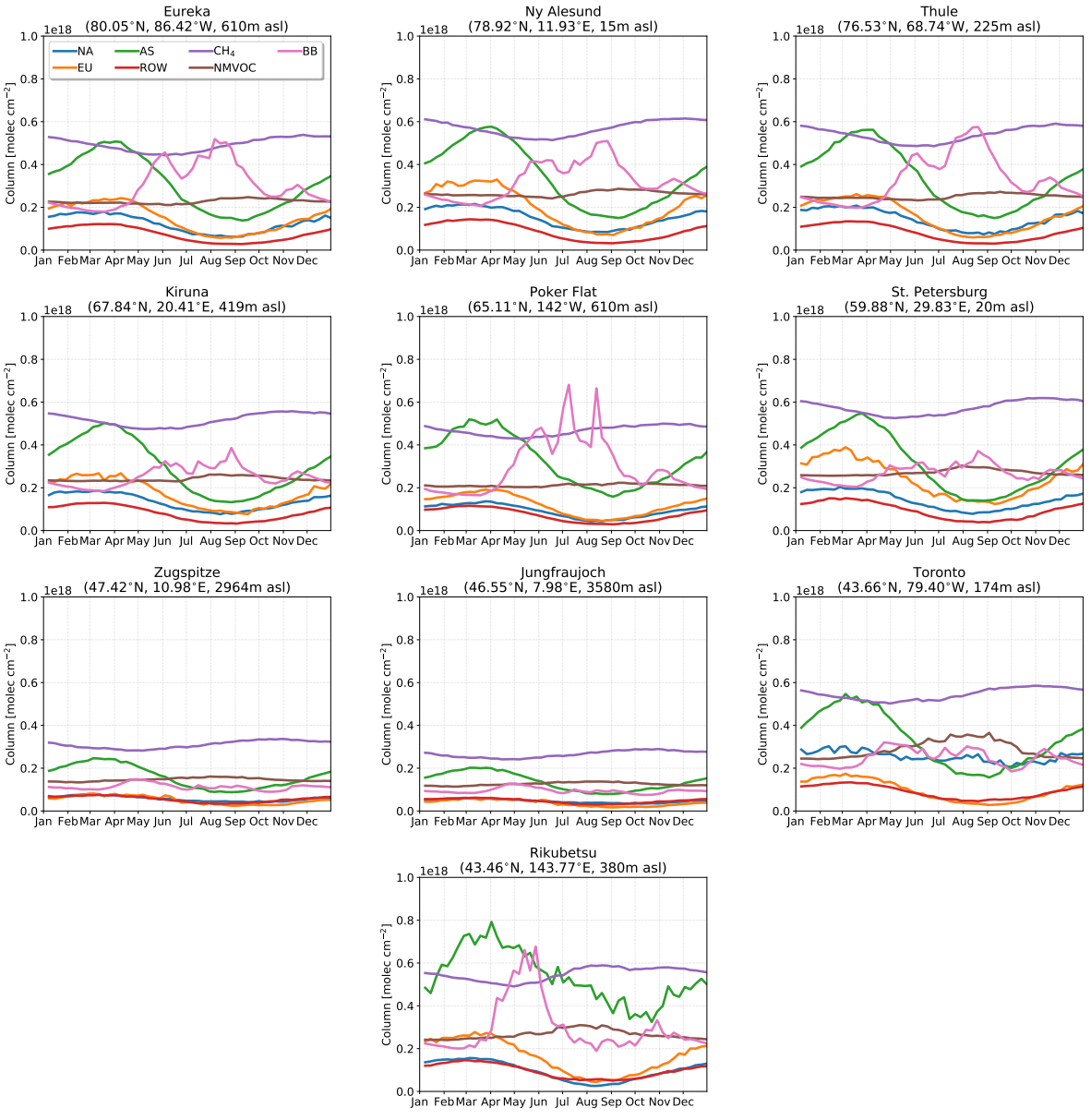

Figure 11. Weekly-mean GEOS-Chem tagged CO tracer tropospheric columns. The tagged CO tracer correspond to those listed in Table 2. The total biomass burning (BB) contribution is shown and is the sum of all biomass burning tracers from Table 2.

https://doi.org/10.5194/acp-2019-881
Preprint. Discussion started: 18 November 2019

Atmospheric Chemistry and Physics Discussions

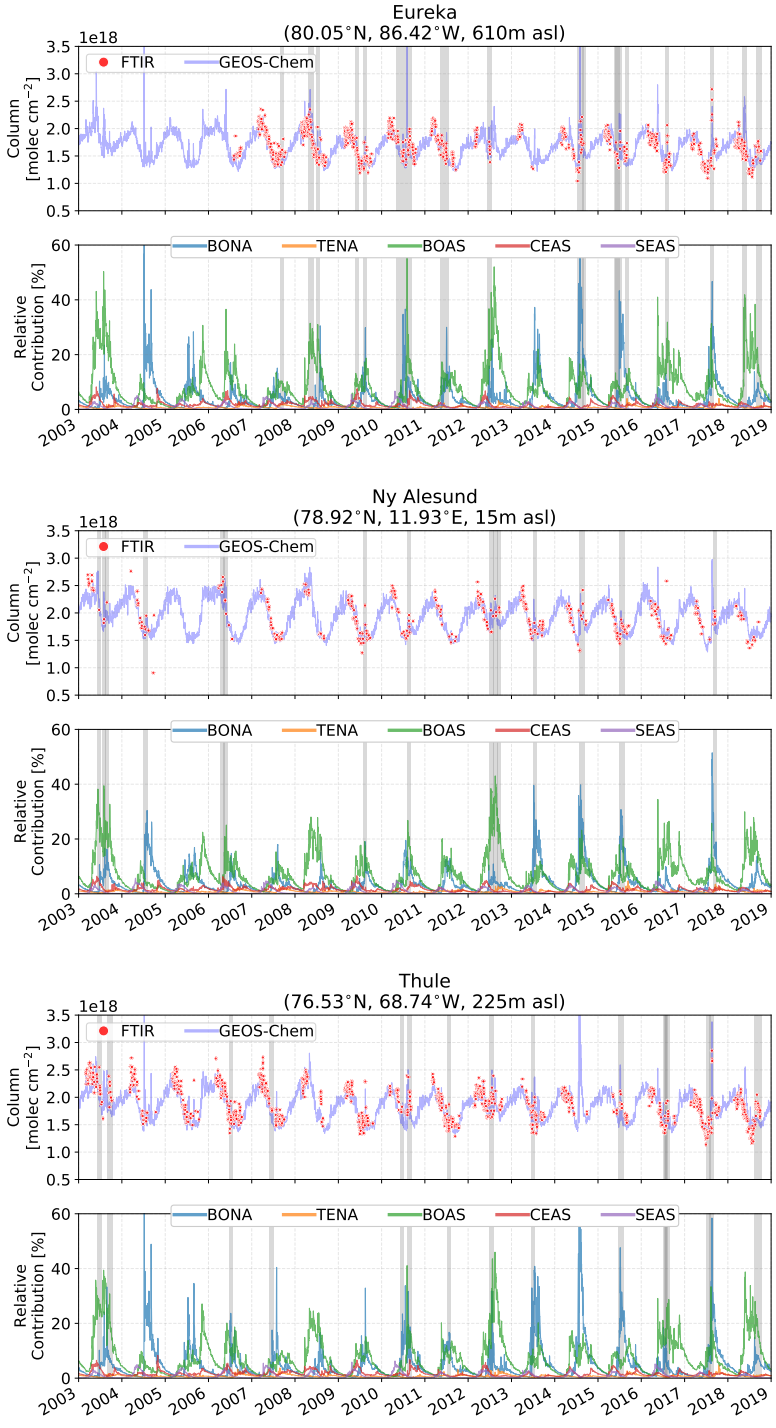

Figure 12. Daily-mean CO tropospheric column time series for FTIR and GEOS-Chem (top panel) from 2003-2018 for the high-Arctic sites: Eureka, Ny-Ålesund and Thule. The bottom panel shows the relative contribution (%) of the BONA, TENA, BOAS, CEAS and SEAS CO tracers in the GEOS-Chem simulation to the total CO tropospheric column. The grey shaded regions indicate periods of fire-affected measurements identified in the FTIR time series and summarized in Figure 10

https://doi.org/10.5194/acp-2019-881
Preprint. Discussion started: 18 November 2019

Atmospheric Chemistry and Physics Discussions

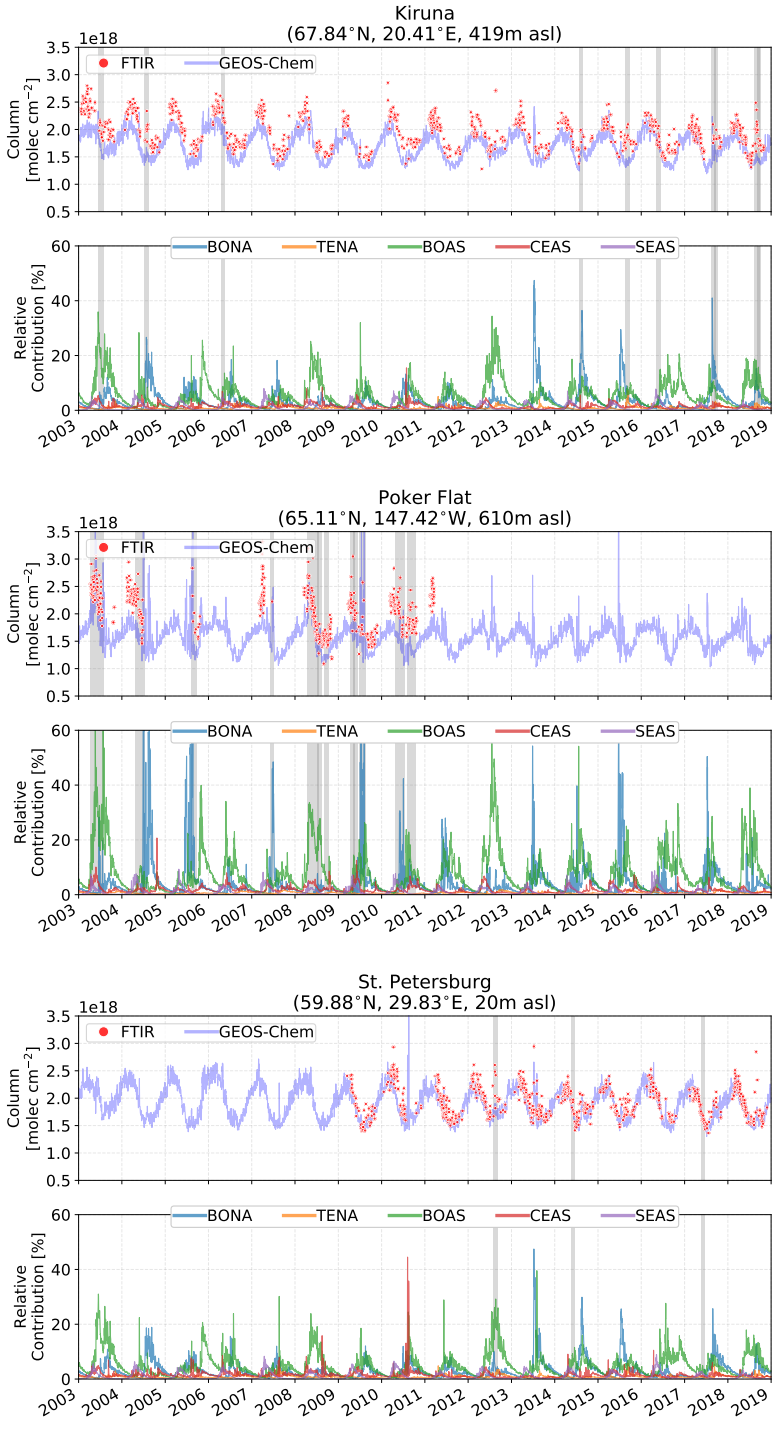

Figure 13. Same as Figure 12 but for the Arctic sites: Kiruna, Poker Flat and St. Petersburg .

https://doi.org/10.5194/acp-2019-881
Preprint. Discussion started: 18 November 2019

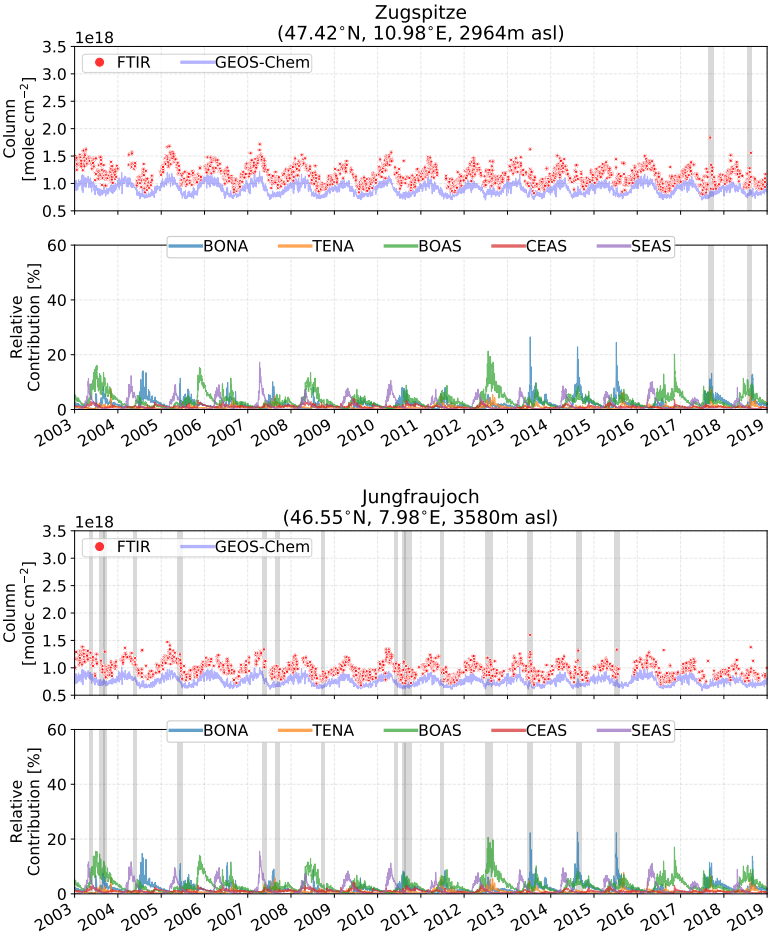

Figure 14. Same as Figure 12 but for the alpine sites: Zugspitze and Jungfraujoch.

https://doi.org/10.5194/acp-2019-881
Preprint. Discussion started: 18 November 2019

Atmospheric Chemistry and Physics Discussions

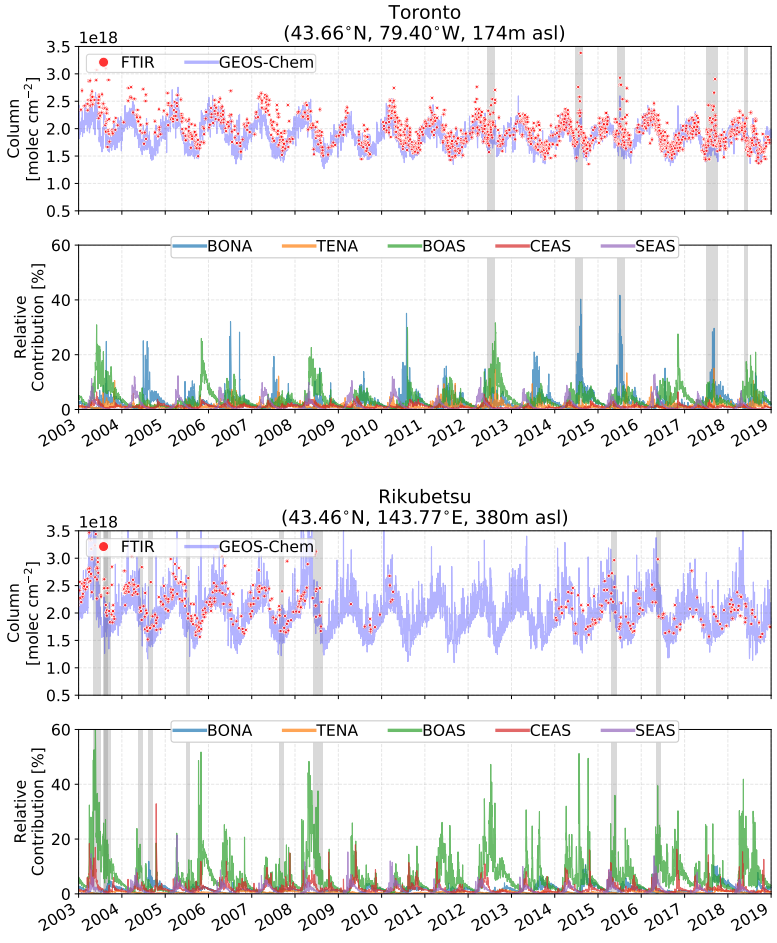

Figure 15. Same as Figure 12 but for the mid-latitude sites: Rikubetsu and Toronto.

https://doi.org/10.5194/acp-2019-881
Preprint. Discussion started: 18 November 2019

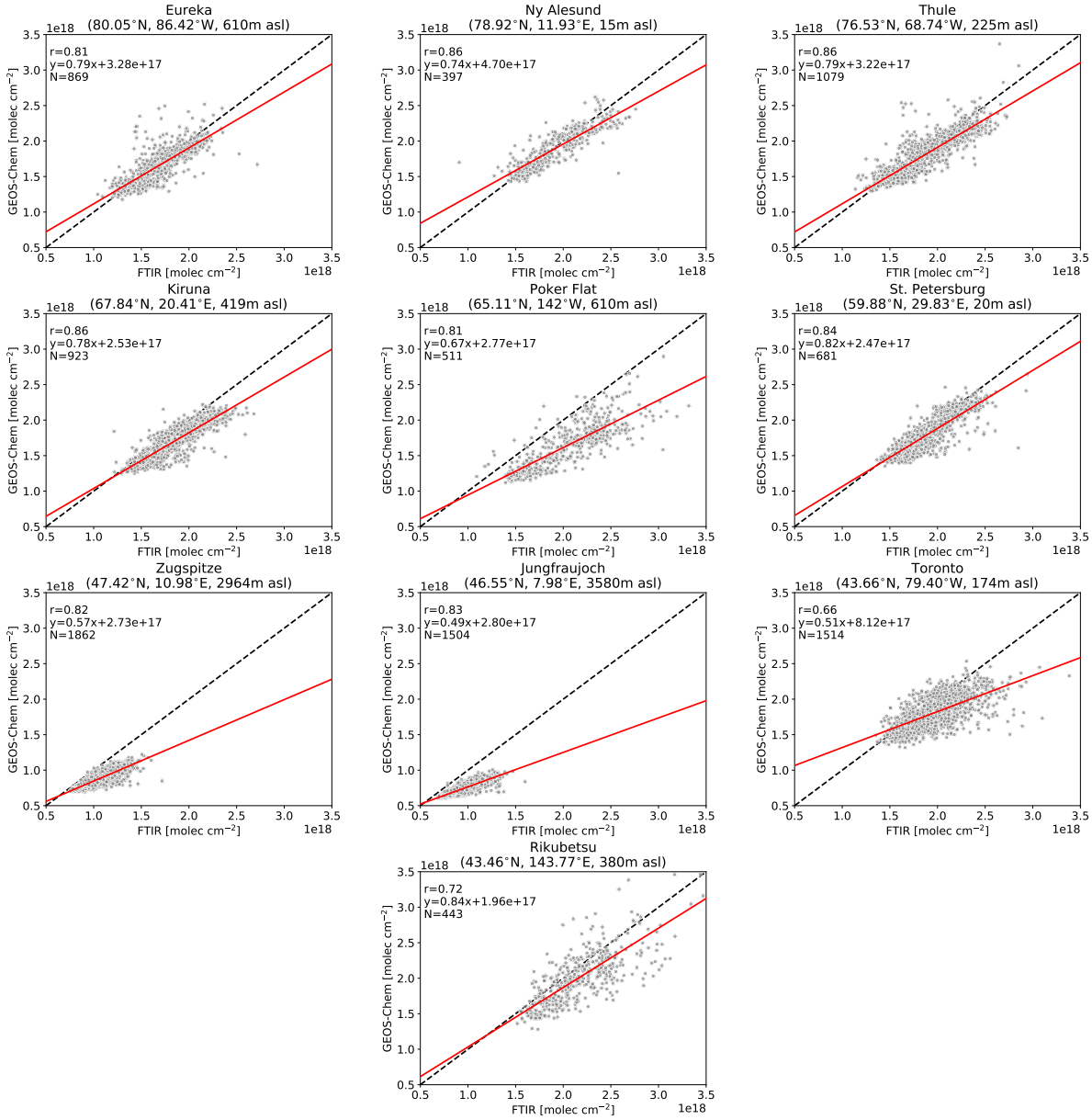

Figure 16. Correlation of daily-averaged GEOS-Chem and FTIR CO tropospheric partial columns for all sites from 2003-2018. The linear correlation coefficient (r), linear equation of the regression, and number of measurements (N) are also shown. The black dashed line is the one-to-one correlation and the solid red line is the fitted linear regression.

https://doi.org/10.5194/acp-2019-881
Preprint. Discussion started: 18 November 2019

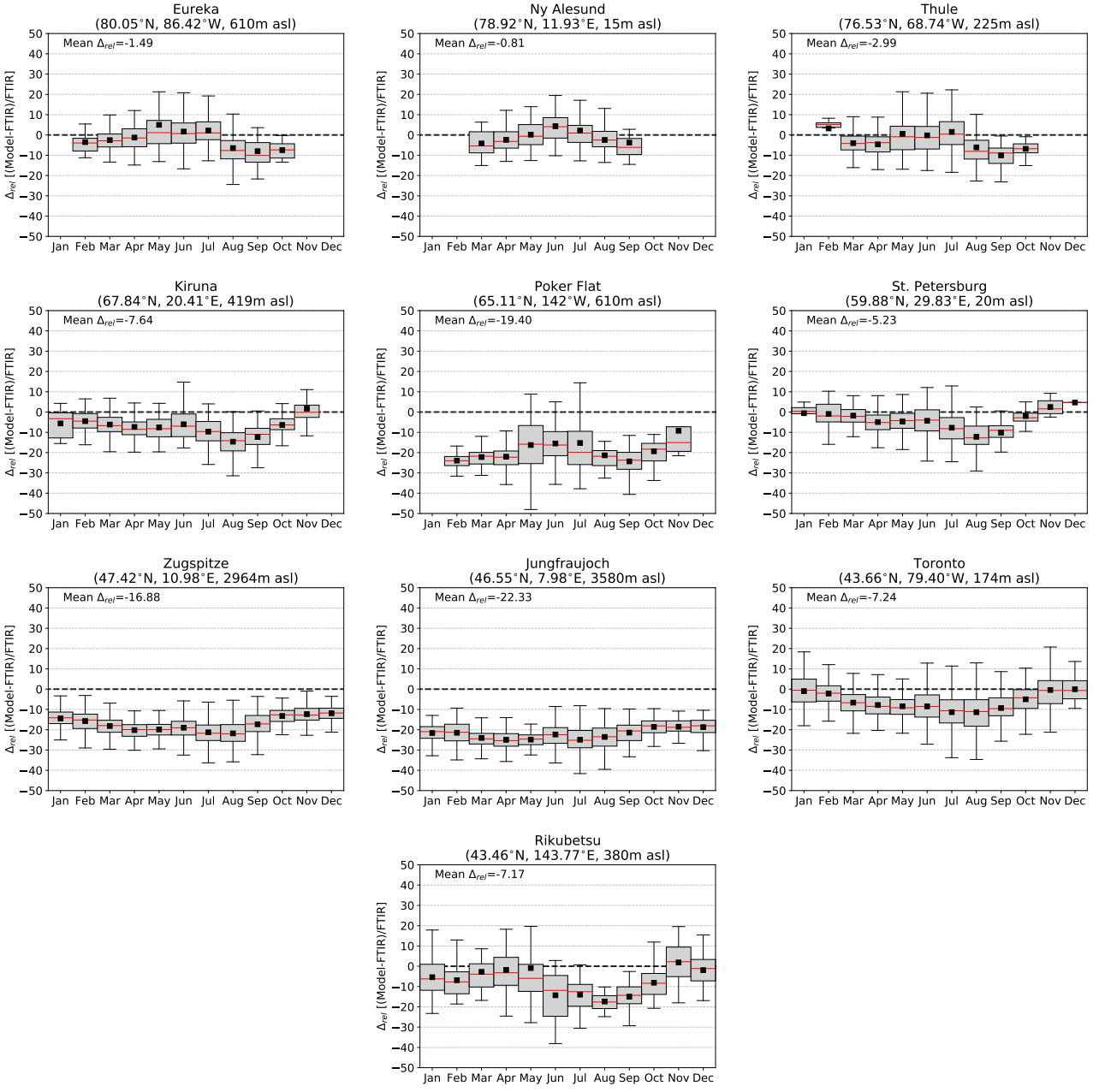

Figure 17. Box-and-whiskers plot of the monthly-mean relative difference (%) of GEOS-Chem and FTIR CO taken over all years from 2003-2018. The red line indicates the mean and the black square is the median. The shaded boxes represent the interquartile range of the data and the whisker represent the range. The mean relative difference of all data is listed in the top left corner.